AD-A181 447 BLUE-GREEN LASER DIODE RESEARCH PROGRAM REVISION(U) 1/1
MINNESOTA MINING AND MFG CO ST PAUL ELECTRONIC AND
INFORMATION SECTOR LAB H A MAR ET AL. MAY 87
UNCLASSIFIED N00014-85-C-0552 F/G 9/3 NL

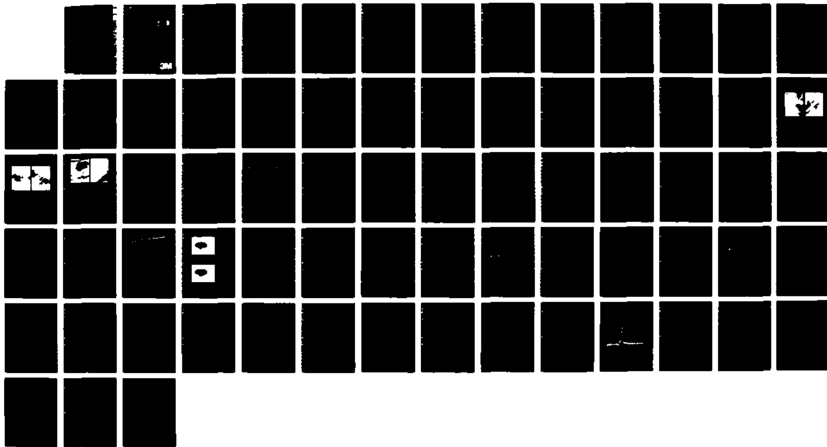

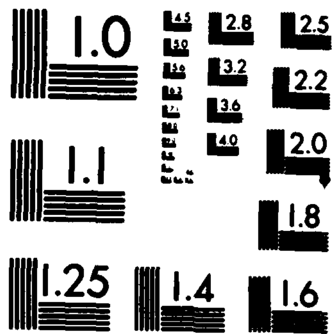

MICROCOPY RESOLUTION TEST CHART
NATIONAL BUREAU OF STANDARDS-1963-A

DTIC FILE COPY

(12)

BLUE-GREEN LASER DIODE RESEARCH PROGRAM

AD-A181 447

Quarterly Technical Progress Report No. 4
For The Period January 1, 1987 To March 31, 1987

DTIC
SELECTED
JUN 1 2 1987
D

Prepared Under
Contract Number N00014-85-C-0552

APRIL, 1987/REVISED MAY, 1987

APPPROVED FOR PUBLIC RELEASE
DISTRIBUTION UNLIMITED

The views and conclusions contained in this document are those of the authors and should not be interpreted as necessarily representing the official policies, either expressed or implied, of the Defense Advanced Research Projects Agency or the U.S. Government.

Work supported in part by the:

DEFENSE ADVANCED RESEARCH PROJECTS AGENCY
1400 Wilson Boulevard
Arlington, VA 22209

Under the:

OFFICE OF NAVAL RESEARCH
Department Of The Navy
800 N. Quincy Street
Arlington, VA 22217-5000

Electronic and Information
Sector Laboratories/3M

St. Paul, MN 55144-1000

3M

87 6 10 134

UNCLASSIFIED

SECURITY CLASSIFICATION OF THIS PAGE

AD-A181447

REPORT DOCUMENTATION PAGE

1a. REPORT SECURITY CLASSIFICATION	1b. RESTRICTIVE MARKINGS
UNCLASSIFIED	
2a. SECURITY CLASSIFICATION AUTHORITY	3. DISTRIBUTION/AVAILABILITY OF REPORT
2b. DECLASSIFICATION/DOWNGRADING SCHEDULE	Approved for Public Release Distribution Unlimited
4. PERFORMING ORGANIZATION REPORT NUMBER(S)	5. MONITORING ORGANIZATION REPORT NUMBER(S)
Quarterly Technical Progress Report No. 4	
6a. NAME OF PERFORMING ORGANIZATION: 3M Company 6b. OFFICE SYMBOL (If applicable)	7a. NAME OF MONITORING ORGANIZATION: Defense Advanced Research Projects Agency
6c. ADDRESS (City, State and ZIP Code) E&I Sector Laboratory - 201-1N-36 3M Center - St. Paul, MN 55144	7b. ADDRESS (City, State and ZIP Code) 1400 Wilson Boulevard Arlington, VA 22209
8a. NAME OF FUNDING/SPONSORING ORGANIZATION: Office of Naval Research 8b. OFFICE SYMBOL (If applicable)	9. PROCUREMENT INSTRUMENT IDENTIFICATION NUMBER Contract No. N00014-85-C-0552
8c. ADDRESS (City, State and ZIP Code) Dept. of the Navy 800 N. Quincy St. Arlington, VA 22217-5000	10. SOURCE OF FUNDING NOS. PROGRAM ELEMENT NO. / PROJECT NO. / TASK NO. / WORK UNIT NO.
11. TITLE (Include Security Classification) Blue-Green Laser Diode Research Program	

12. PERSONAL AUTHOR(S)
Drs. H.A. Mar, T.L. Smith, and C.T. Walker

13a. TYPE OF REPORT	13b. TIME COVERED	14. DATE OF REPORT (Yr., Mo., Day)	15. PAGE COUNT
Technical Progress	FROM 87/01/01 TO 87/03/31	1987, April/Rev. May	69

16. SUPPLEMENTARY NOTATION

17. COSATI CODES			18. SUBJECT TERMS (Continue on reverse if necessary and identify by block number)
FIELD	GROUP	SUB. GR.	Blue-Green Laser or Lasers, Blue-Green

19. ABSTRACT (Continue on reverse if necessary and identify by block number)

During this reporting period, Na-doping work continued, and, in addition, work began with P- and Sb-doping. The laboratories also began to use a new 6N super high-purity Se source material obtained from Osaka Asahi, with consequent marked improvement in unintentionally-doped material quality. As evident from this report, extrinsic donor impurities from the source materials may be responsible for the difficulties encountered in obtaining p-ZnSe. Efforts in double-crystal x-ray rocking curve (DCRC) and transmission electron microscopy studies, as well as e-beam and optical pumping, and Schottky and ohmic contact work are continuing.

20. DISTRIBUTION/AVAILABILITY OF ABSTRACT	21. ABSTRACT SECURITY CLASSIFICATION
UNCLASSIFIED/UNLIMITED ☐ SAME AS RPT. ☒ DTIC USERS ☐	UNCLASSIFIED

22a. NAME OF RESPONSIBLE INDIVIDUAL	22b. TELEPHONE NUMBER (Include Area Code)	22c. OFFICE SYMBOL
L.C. McGraw	(612) 733-9816	

DD FORM 1473, 83 APR EDITION OF 1 JAN 73 IS OBSOLETE.

UNCLASSIFIED

SECURITY CLASSIFICATION OF THIS PAGE

EXECUTIVE SUMMARY

In the previous Quarterly Technical Progress Report, there was increased emphasis on efforts to incorporate acceptors in ZnSe. The St. Paul group concentrated on Na-doping, while the Toronto group directed its efforts to N-doping. In this quarter, Na-doping work has continued, and, in addition, work has begun with P- and Sb-doping in St. Paul and Toronto, respectively. Both laboratories have now begun to use a new 6N super high-purity Se source material obtained from Osaka Asahi, with consequent marked improvement in unintentionally-doped material quality. As will be evident from this report, extrinsic donor impurities from the source materials may be responsible for the difficulties encountered in obtaining p-ZnSe. Efforts in double-crystal x-ray rocking curve (DCRC) and transmission electron microscopy studies in Toronto, as well as e-beam and optical pumping, and Schottky and ohmic contact work in St. Paul, are continuing.

It has been suggested in the literature that the difficulty in obtaining p-ZnSe is based on thermodynamics. If this is true, it may be that p-ZnSe will never be obtained. However, there have also been suggestions that the difficulty is not entirely thermodynamic in nature, and indeed may primarily be one of compensation by donor impurities. In Quarterly Technical Progress Report No. 3, we reported the results of preliminary studies on Na-doping that showed increasing free electron concentrations with increasing Na_2Se cell temperatures. Although donor-acceptor pair emission was observed in the PL measurements, there were only weak indications of an acceptor bound exciton peak. In order to determine the extent of Na incorporation in the ZnSe and to identify donor impurities (which earlier results alluded to above suggest may be present), SIMS measurements were performed on a number of Na-doped samples.

The results of SIMS analyses show that in both undoped and doped samples, significant contamination with such impurities as As, Cu, Fe, Ni and probably other elements is present. Additionally, the Na-doped samples showed heavy K contamination; in fact, the K concentration was comparable to that of Na. This data, in conjunction with SIMS and Hall data which show that in doping experiments the free electron concentration increases by over an order of magnitude before Na incorporation begins, suggest that the

Avail and/or Special
A-1

effects of intentional doping are being obscured by the presence of unintentional impurities.

In addition to the Na-doping experiments, preliminary studies were begun on P- and Sb-doping of the ZnSe layers. Zn_3P_2 was used as the source of P and elemental material was used for Sb-doping. As in the case of the Na_2Se source, PL and electrical measurements suggest that large concentrations of donor impurities are being incorporated in the ZnSe from the source Zn_3P_2 material. The results also suggest that although small concentrations of P give rise to a shallow acceptor level, higher concentrations give rise to a deep acceptor level. With regard to Sb-doping, although the results of PL and electrical measurements are still inconclusive, SIMS analysis indicates very low Sb incorporation ($\sim 7.3 \times 10^{16} cm^{-3}$), even though Sb beam pressures as high as 10^{-9} mbar (Zn, Se beam pressures are $\sim 2 \times 10^{-6}$ mbar) are being used. It is interesting to note that Auger spectra of the heavily doped ZnSe layers show the presence of Sb; this implies surface concentrations far in excess of the "bulk" concentration and suggests a high sticking coefficient but low bulk incorporation.

Studies are continuing on the e-beam pumping of OMVPE material provided by Prof. B. Wessels of Northwestern University. Thresholds for cavities produced from the OMVPE material are about 2.5X to 10X higher than those produced from MBE-grown material. Techniques are being developed to evaporate metal mirrors onto the end facets of the laser cavity to reduce lasing thresholds.

The DCRC comparative analysis of the ZnSe/(100) Ge and ZnSe/(100) GaAs systems reported in Quarterly Technical Progress Report No. 3 continued this quarter. It showed that in spite of the fact that the mismatch in the ZnSe/Ge system is smaller than that of the ZnSe/GaAs system, the ZnSe layer quality, as determined by PL and DCRC linewidths, was better in the latter case. It is shown here that the anomaly is due to dislocations propagating throughout the ZnSe in the ZnSe/Ge system, whereas they are confined to within 0.5 μm of the interface in the ZnSe/GaAs system. In addition, because the tilt of the ZnSe lattice with respect to substrate lattice is

greater for the ZnSe/Ge system, it is suggested that there may be a relationship between large tilt and dislocation propagation in the ZnSe.

Cross-sectional and planar transmission electron microscopy studies performed on the ZnSe/Ge and ZnSe/GaAs system confirm the results obtained by the DCRC and PL studies. Indeed, the planar studies showed the presence of a cellular structure in ZnSe/Ge with each cell delineated by low-angle grain boundaries.

TABLE OF CONTENTS

Section **Page**

1.0 INTRODUCTION.. 1

2.0 PROGRESS REPORT.. 2
2.1 Project 1, Task 1: Materials Research - Undoped ZnSe Research. 2
2.1.1 Unintentionally-Doped ZnSe Heteroepitaxy on (100) GaAs.. 2
2.1.1.1 Growth of Unintentionally-Doped ZnSe on (100) GaAs.. 2
2.1.1.2 Photoluminescence of Unintentionally-Doped ZnSe on (100) GaAs.. 3
2.1.1.3 Selective Excitation Photoluminescence of ZnSe on (100) GaAs.. 5
2.1.2 X-Ray and Photoluminescence Comparative Studies of ZnSe/(100) GE and ZnSe/(100) GaAs.. 8
2.1.2.1 Double-Crystal X-Ray Analysis.. 8
2.1.2.2 Photoluminescence Analysis.. 15
2.1.3 Cross-Sectional and Planar Transmission Electron Microscopy: Defect Characterization of ZnSe/(100) Ge, ZnSe/(100) GaAs and ZnSe/(211) Ge.. 16
2.1.3.1 ZnSe/(211) Ge.. 17
2.1.3.2 ZnSe/(100) Ge.. 17
2.1.3.3 ZnSe/(100) GaAs.. 18
2.2 Project 1, Task 2: Materials Research - p-ZnSe.. 21
2.2.1 Na-Doped ZnSe on (100) GaAs.. 21
2.2.1.1 Na-Doped ZnSe: Growth and SIMS Characterization.. 21
2.2.1.2 Na-Doped ZnSe: Photoluminescence.. 26
2.2.1.3 Na-Doped ZnSe: Electrical Characterization.... 28
2.2.2 Sb-Doped ZnSe on (100) GaAs.. 32
2.2.2.1 Sb-Doped ZnSe: Growth and SIMS Characterization.. 32
2.2.2.2 Sb-Doped ZnSe: Photoluminescence.. 36
2.2.2.3 Sb-Doped ZnSe: Electrical Measurements........ 39
2.2.3 P-Doped ZnSe on (100) GaAs.. 39
2.2.3.1 P-Doped ZnSe: Growth.. 40
2.2.3.2 P-Doped ZnSe: Photoluminescence.. 41
2.2.3.3 P-Doped ZnSe: SIMS Characterization........... 45
2.2.3.4 P-Doped ZnSe: Electrical Characterization..... 46
2.3 Project 2, Task 1: Device Research - Photopumping, e-Beam Pumping and Cavity Formation.. 52
2.3.1 e-Beam Pumping Measurements.. 52
2.4 Project 2, Task 2: Contact Studies.. 55
2.4.1 Electron Transport Across GaAs-ZnSe Interface........... 55

3.0 REFERENCES.. 61

LIST OF FIGURES

Figure		Page
2-1.	Photoluminescence and selective excitation photoluminescence measurements for samples grown with different Se starting material	4
2-2.	Variations in SPL spectra with growth parameter and starting material	6
2-3.	TEDS region of ZSE88A showing the presence of Cl, Ga, In and F	7
2-4.	Energies of the observed peaks associated with Cl, Ga, In, and F plotted as a function of laser energy	9
2-5.	Resonance behaviors of the In 2S and 2P RS peaks as well as the F TEDS line are observed	10
2-6.	Double-crystal rocking curve (DCRC) (400) linewidth data recorded from ZnSe/(100) GaAs and ZnSe/(100) Ge layers grown under a fixed set of growth conditions to various thicknesses	11
2-7.	(a) Layer/substrate (400) peak angular separation plotted as a function of rotation angle for a typical ZnSe/GaAs sample, (b) Bragg reflection model for the ZnSe/GaAs sample	13
2-8.	(a) Layer/substrate (400) peak angular separation plotted as a function of rotation angle for a typical ZnSe/Ge sample, (b) Bragg reflection model for the ZnSe/Ge sample	14
2-9.	Donor-Bound Exciton (DBE) linewidth data obtained from 4.2K PL measurements of ZnSe/GaAs and ZnSe/Ge layers grown to various thicknesses under a fixed set of growth conditions	15
2-10.	Transmission Electronic Microscopy images of ZnSe/(211) Ge sample in (a) cross-sectional view and (b) planar view	17
2-11.	Transmission Electron Microscopy images of ZnSe/(100) Ge sample in (a) cross-sectional and (b) planar view	18
2-12.	Transmission Electron Microscopy images of ZnSe/(100) GaAs sample in (a) cross-sectional and (b) planar view	19
2-13.	Auger spectrum of a Na-doped ZnSe/Si sample showing a prominent K peak	22
2-14.	Carrier concentration plotted as a function of beam pressure ratio for two growth temperatures. Na concentrations determined by SIMS are indicated	30
2-15.	(a) Carrier concentrations and peak mobilities for various growth temperatures with BPR 1:1. (b) Carrier concentrations and peak mobilities for various growth temperatures with BPR 1/2:1	31
2-16.	Auger spectra of (a) undoped and (b) Sb-doped ZnSe layers. Note the Sb peak is present indicating very high Sb surface concentrations	34

LIST OF FIGURES (continued)

Figure **Page**

2-17. RHEED pattern of the undoped ZnSe along the [1$\bar{1}$0] azimuth showing 1/2-order reconstruction. The pattern is intensified when the Sb-shutter is opened 35

2-18. (a) 4.2K PL spectrum of undoped ZnSe/(100) GaAs growth using the 6N+ Se source. (b) Shows the free exciton peak dominates the spectrum 37

2-19. (a) 4.2K PL spectrum of the most heavily Sb-doped layer. The only significant new peak when compared with that of the undoped material is I_1 shown in greater detail in (b) 38

2-20. Auger spectrum of Zn_3P_2-coated Si substrate 40

2-21. 9K PL spectra showing a dramatic increase in the deep level emission in changing T_g from 350°C to 250°C 44

2-22. Plot of the P concentration versus the reciprocal growth temperature 47

2-23. Room temperature electron concentration plotted as a function of Zn_3P_2 oven temperature 48

2-24. Carrier concentration and peak mobility of P-doped layers plotted as a function of BPR for constant T_g and P flux 50

2-25. Carrier concentration and peak mobility of P-doped layers plotted as a function of T_g for constant BPR and P flux 51

2-26. Light output of e-beam pumped laser versus e-beam current density .. 53

2-27. No correlation between large NBE emission intensity and small lasing threshold is seen in this plot of light output versus e-beam current 54

2-28. At low e-beam current densities, the Cl spectra for both ZSE88A and ZSE48A are dominated by a feature believed to be due to inelastic scattering of excitons by electrons (446 nm peak) 56

2-29. Current-voltage characteristics of gold Schottky barriers on ZnSe .. 58

2-30. Current-voltage characteristics of indium (ohmic) and gold (Schottky) contacts to ZnSe with current transport through n^+-GaAs and n-ZnSe interface 60

LIST OF TABLES

Table Page

2-1. Samples for O_2^+ SIMS Comparative Analyses 23

2-2. SIMS Positive Secondary Ion Spectra 24

2-3. Depth Profile Analysis Results 25

2-4. Na_2Se Doping 27

2-5. Sb-Doping Parameters 36

2-6. Zn_3P_2 Doping, $T(Zn_3P_2) = 500°C$ 42

2-7. Zn_3P_2 Doping, $T(Zn_3P_2) = 450°C$ 43

2-8. P-Doping Parameters 46

1.0 INTRODUCTION

This report covers progress during the sixteenth through eighteenth months of ONR Contract N00014-85-C-0552. The various sections of the report are numbered and titled using the format of the original proposal. As before, results from parallel programs at 3M-St. Paul and 3M-Toronto are discussed.

2.0 PROGRESS REPORT

2.1 Project 1, Task 1: Materials Research - Undoped ZnSe Research

This quarter, both the St. Paul and the Toronto groups continued to expend some effort in the growth of high-quality unintentionally-doped ZnSe. A new, very high-purity Se source material was obtained and its effects on ZnSe layer quality were characterized by both groups. In addition, work continues on characterizing the layers by double-crystal x-ray diffractometry, planar and cross-sectional transmission electron microscopy, Hall mobility and capacitance spectroscopy, e-beam pumping, and PL studies.

2.1.1 Unintentionally-Doped ZnSe Heteroepitaxy on (100) GaAs

2.1.1.1 The Growth of Unintentionally-Doped ZnSe on (100) GaAs

So far all the unintentionally-doped ZnSe samples grown on (100) GaAs substrates have n-type conductivity with electron concentrations from mid-10^{15} to low-10^{17} cm^{-3}. The concentrations of possible group III substitutional impurities (such as Al, Ga, and In) in the samples were determined by SIMS measurement not to be able to account for the carrier concentrations. This leaves the possible sources of shallow donor levels to be either group VII elements or intrinsic defects. However, it is very difficult to measure the concentration of group VII elements, especially F and Cl, in the sub-part-per-million range by any technique. A reasonable way to further sort out the true source of the donor levels is to use starting materials from different vendors because different refining processes may lead to different contaminants.

Residual impurities in the Zn and Se starting materials, rather than native defects, are suspected to be the primary source of unintentional donors (and acceptors) in our undoped ZnSe films. To test this hypothesis, three samples were grown under identical conditions (BPR=1/2:1, T_g=350) using three different sources of Se. ZSE67A was grown using Se purchased from SPEX industries; ZSE74A was grown using Se obtained from ALPHA; and ZSE77A was grown using ultra-pure Se obtained from OSAKA ASAHI METALS. The room temperature carrier concentrations and peak mobilities determined for these three samples are:

SAMPLE	n_{300} (cm^{-3})	μ(cm^2/v-sec)
ZSE67A	$2x10^{16}$	4000
ZSE74A	$5.5x10^{15}$	6800
ZSE77A	$< 1x10^{14}$	not measurable

These results show that the electrical characteristics of each film depend on the Se source material. The Se used for each of these films was specified to be greater than 99.999% pure on a total metals basis; however, non-metallic impurity content could vary depending upon the vendors purification procedure. From these measurements we suspect that the inadvertent doping occurring in our earlier ZnSe epitaxial films was largely due to the non-metallic impurity content of the Se starting material. Cl is one possible major contaminant since it is very difficult to remove $SeCl_4$ using standard distillation techniques.

2.1.1.2 Photoluminescence of Unintentionally-Doped ZnSe on (100) GaAs

During the past quarter, we measured the photoluminescence spectra for MBE-grown samples ZSE74-96, and have performed selective excitation PL (SPL) measurements on several of these samples. Two major developments ensued from these studies and will be discussed below.

Sample ZSE74 was grown at our standard "check run" conditions (T_g=350°C, BPR=1/2:1) but using new Se from Alpha Chemicals. The PL spectrum was quite similar to that observed in the past when we used SPEX Se. Similarly, sample ZSE77 was grown using new ultra-pure 6N+ Se from Osaka Asahi. It shows a radically different PL spectrum. Figure 2-1(a) compares the PL spectra for samples ZSE74 and 77. While the free-exciton emission in ZSE77 was reduced by 4X, the most noticeable difference lies in the region of the donor-bound exciton emission. There the I_2 and I_x peaks were reduced by X20, going from ZSE74 to ZSE77. This decrease was reflected in the electrical measurements which showed an approximate 100X decrease in the (electron) carrier concentrations. Together, these observations constitute the strongest evidence we have seen for the conclusion that the origin of the donors in unintentionally-doped ZnSe is extrinsic impurities. The near elimination of these extrinsic donors from our starting material gives us cause for optimism in our p-doping efforts. SPL measurements on these two samples [Figure 2-1(b)] show similar two-electron donor satellite (TEDS) spectra when the excitation energy is coincident with the I_{20} peak.

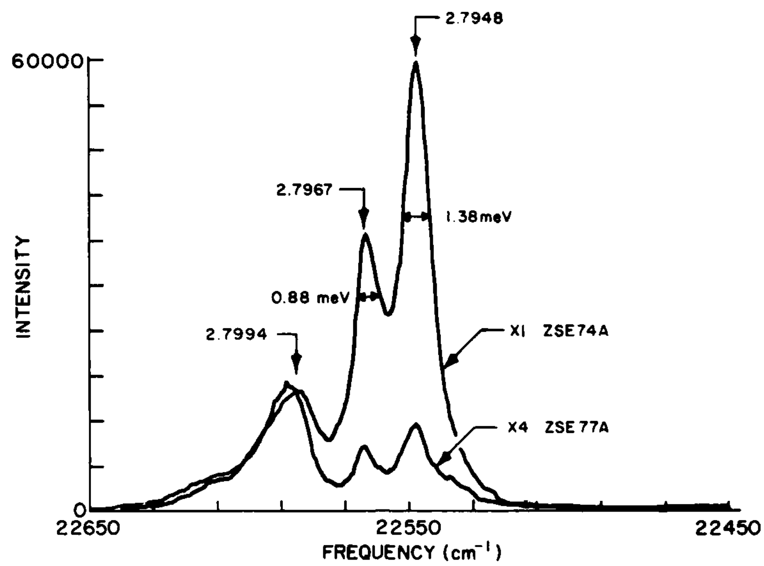

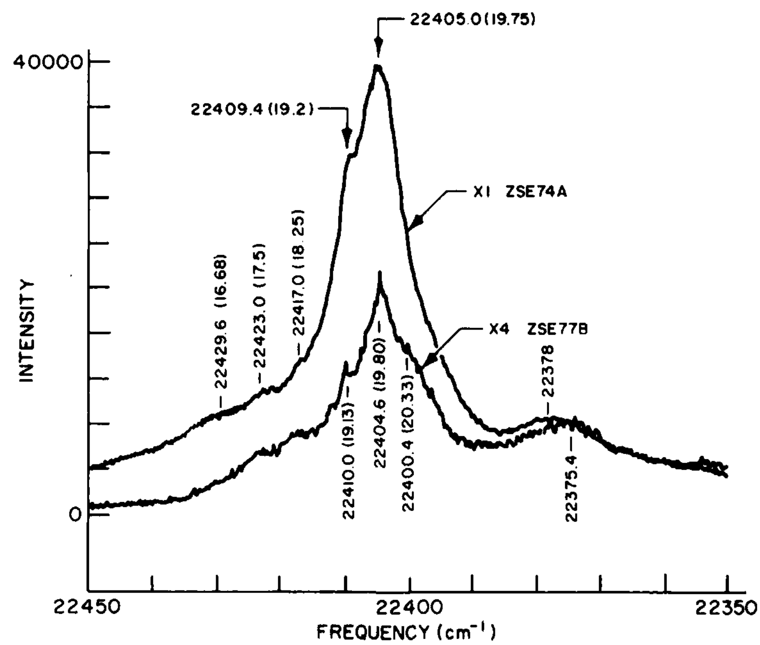

Figure 2-1. Photoluminescence and selective excitation photoluminescence measurements for samples grown with different Se starting material.

The ZSE77 SPL spectrum is 8X weaker than that of ZSE77, for the same excitation conditions, but the spectral features are similar in the two cases.

The spectra are dominated by a broad (1.2 meV) peak due to Cl donors [19.3 and 19.8 meV shift from $E(I_{20})$]; there may be some hint of Ga at 20.3 meV on the high-energy side of the Cl peak in the ZSE77 spectrum.

2.1.1.3 Selective Excitation Photoluminescence of ZnSe on (100) GaAs

We are performing almost routine checks of the SPL spectra of the samples that we are growing in an attempt to identify the major donor species. Figure 2-2 gives some idea of the types of variations observed. The five samples studied here (ZSE37,74, 77,88,93) are all unintentionally-doped and all have narrow (approximately 1 meV, or less) DBE linewidths. However, their TEDS (and/or Raman scattering) spectra differ significantly. Each spectrum in Figure 2-2 was recorded with the dye laser set on the I_{20} peak for that sample. We observed:

ZSE37A "high-quality" film from our growth-matrix study
  -dominant Ga TEDS, some narrow Cl RS.

ZSE74A after changing to Alpha Se
  -strong, broad Cl peak

ZSE77A after changing to 6N+ Se
  -much weaker TEDS; broad Ga, narrower Cl.

ZSE88A after changing to zone-refined Zn; thick(4.75 μm) film.
  -weak TEDS; broad F TEDS; weaker and narrower In;
  also some Cl and Ga.

ZSE93A same as #88 except 1:1, 300°C rather than 1/2:1, 350°C and thinner film.
  -weak TEDS; broad Ga TEDS, weaker, narrower Cl.

These SPL measurements aid the SIMS measurements by pointing to specific donors to probe as suspected contaminants. In addition, it appears that SPL may be able to detect some of these impurities at levels that are below the SIMS detectability limits.

More extensive SPL measurements have been performed on sample ZSE88A (see Figure 2-3). The TEDS region (Figure 2-3) shows several easily-identified species when the excitation energy is at I_{20}.

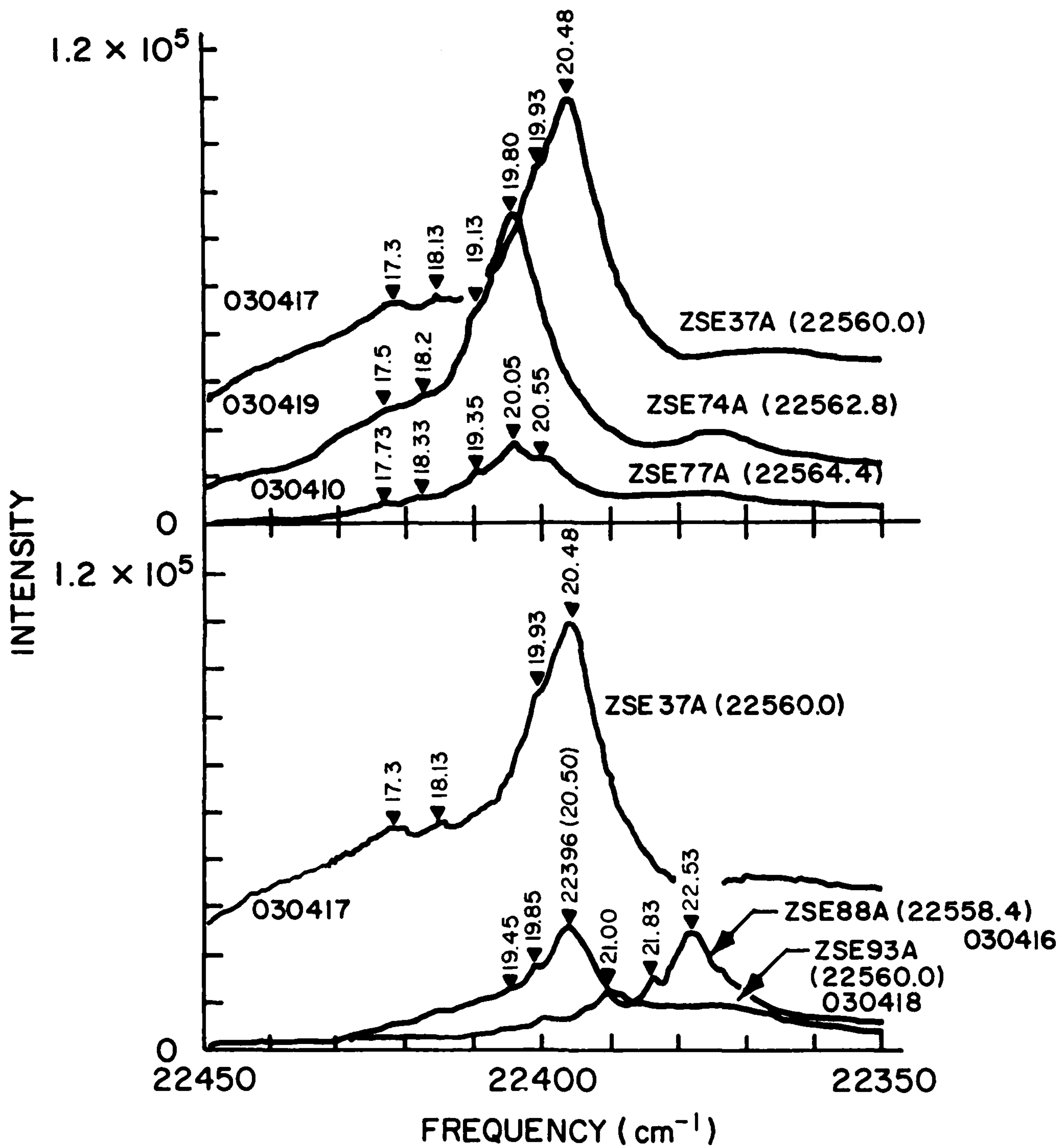

Figure 2-2. Variations in SPL spectra with growth parameter and starting material.

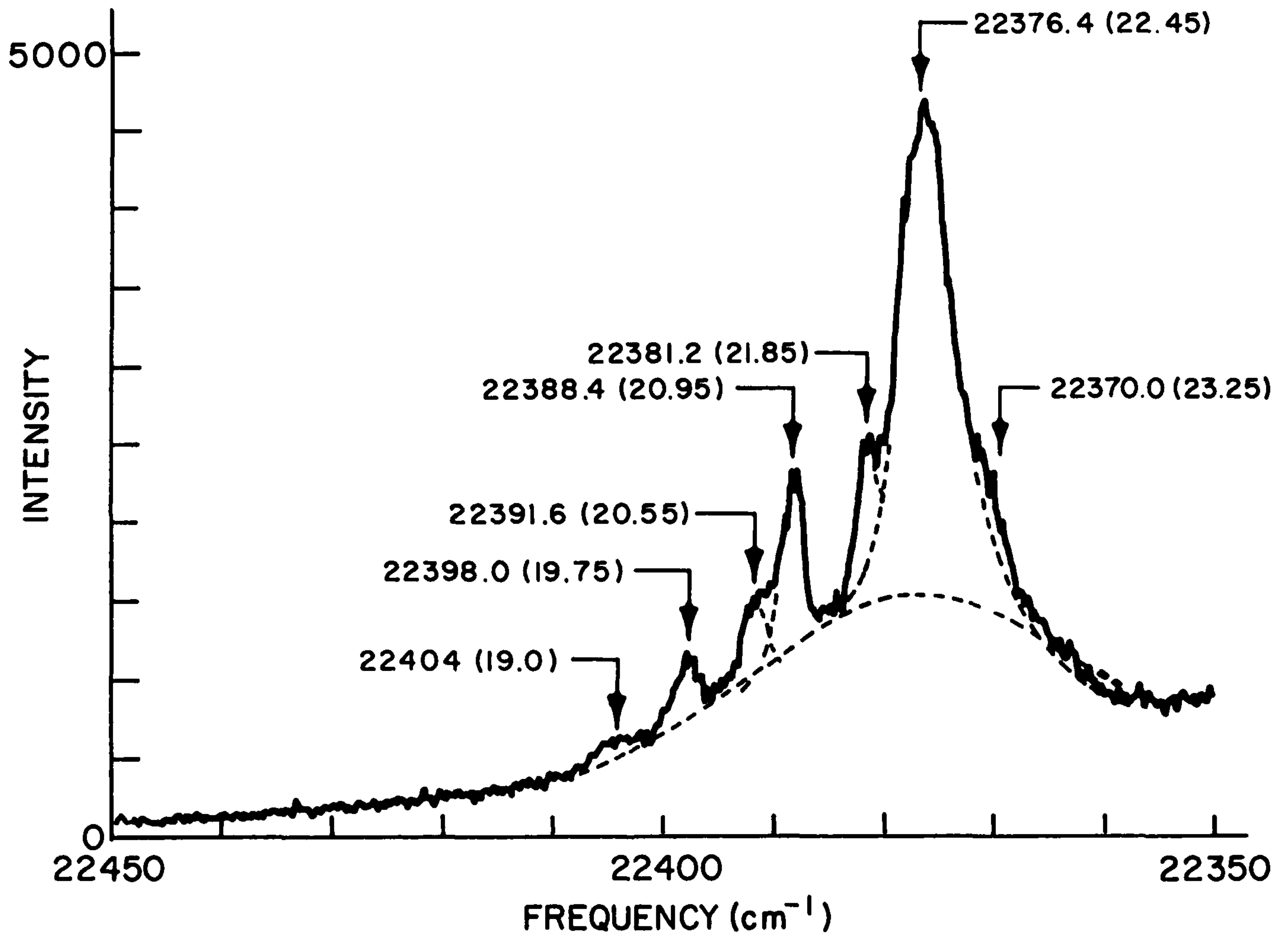

Figure 2-3. TEDS region of ZSE88A showing the presence of Cl, Ga, In, and F.

Narrow peaks due to Cl (19.75 meV), Ga (20.55), In (20.95, 21.85) and F (22.45) are observed under these conditions. The energies of the observed peaks are plotted versus laser energy in Figure 2-4.

With the exception of the F peak which behaves as a TEDS (PL) feature, all the other features behave as Raman scattering. The resonance behavior of the In 2S and 2P RS peaks, as well as the F TEDS line, is displayed in Figure 2-5. While the RS peaks are enhanced near the free exciton and DBE energies, the TEDS line is only strongly enhanced near I_x and I_{20}. These results are similar to those which we have observed previously (see our discussion of sample ZSE37A in a previous report), except that in this sample the major contaminants apprear to be F and In.

2.1.2 X-Ray and Photoluminescence Comparative Studies of ZnSe/(100)Ge and ZnSe/(100) GaAs

In Quarterly Technical Report No. 3 for the period October 1 to December 31, 1986, we reported that careful DCRC analysis of both ZnSe/(100) GaAs and ZnSe/(100) Ge with a substrate surface orientation 2° off (100) → [110] showed that (1) the DCRC linewidths are a function of the thickness of the layer, and (2) the ZnSe layers are misoriented with respect to the substrate. Since then, further analysis was done on the DCRC and PL measurements of the layers and the results are presented and discussed below.

ZnSe layers were grown by the MBE technique to various thicknesses in the range 1 μm to 6.5 μm on both (100) GaAs and (100) Ge substrates using a fixed set of growth conditions, namely a Zn to Se beam pressure ratio of unity together with a substrate temperature of 330°C. Of particular concern in this study were the measured DBE and DCRC linewidths from the ZnSe layers.

2.1.2.1 Double-Crystal X-Ray Analysis

X-ray double-crystal rocking curves are frequently used to assess heteroepitaxial layers. Lattice parameter differences between layer and substrate can be deduced from the angular separation of their diffraction peaks. In addition, the linewidth of the layer diffraction peak is often used as a qualitative indication of layer quality.

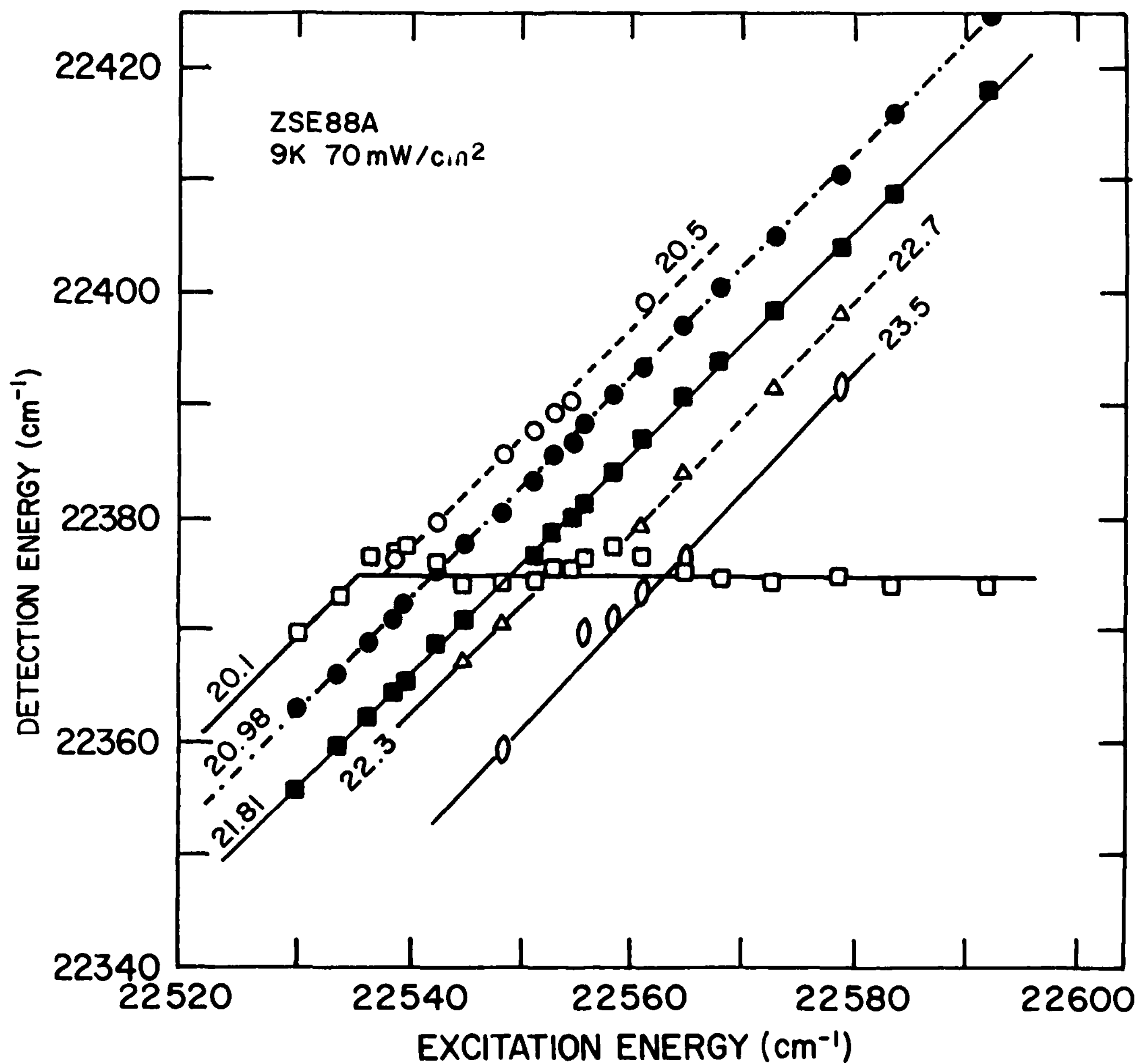

Figure 2-4. Energies of the observed peaks associated with Cl, Ga, In, and F plotted as a function of laser energy.

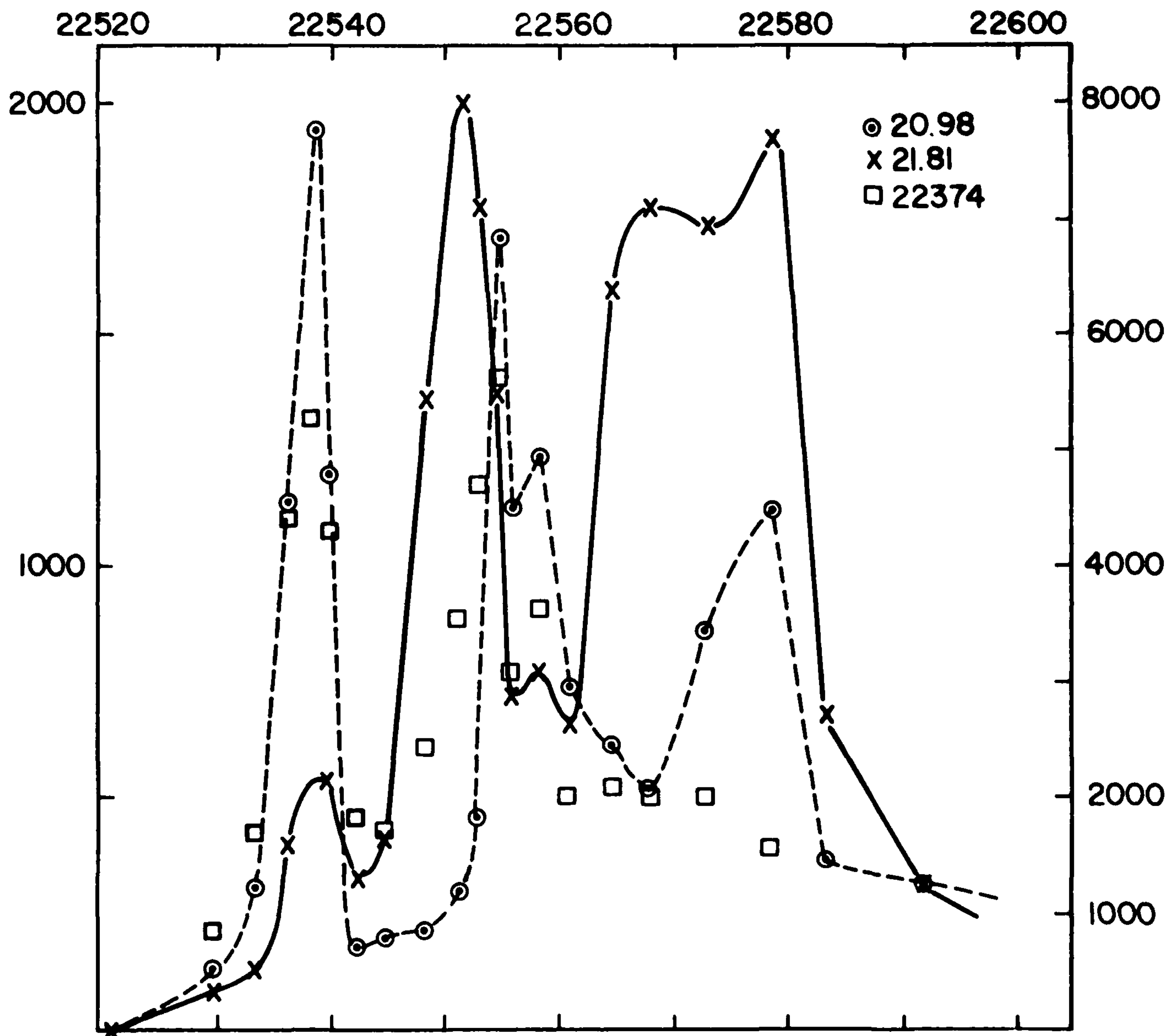

Figure 2-5. Resonance behavior of the In 2S and 2P RS peaks as well as the F TEDS line are observed.

The full width at half maximum of the (400) reflection is most commonly used for the purpose of assessing crystalline perfection. DCRC peak linewidths recorded from heteroepitaxial layers are broadened from those which would be obtained from "perfect" crystals. This is due to lattice distortion in the layers arising from structural phenomena including strain, bending, and dislocations due to non-perfect lattice and thermal expansion coefficient matching with substrate materials.

In this study, DCRC (400 reflection) linewidths were recorded from ZnSe/GaAs and ZnSe/Ge layers grown to various thicknesses under a fixed set of growth conditions; namely, a Zn to Se beam pressure ratio of unity together with a substrate temperature of 330°C. The results are illustrated in Figure 2-6.

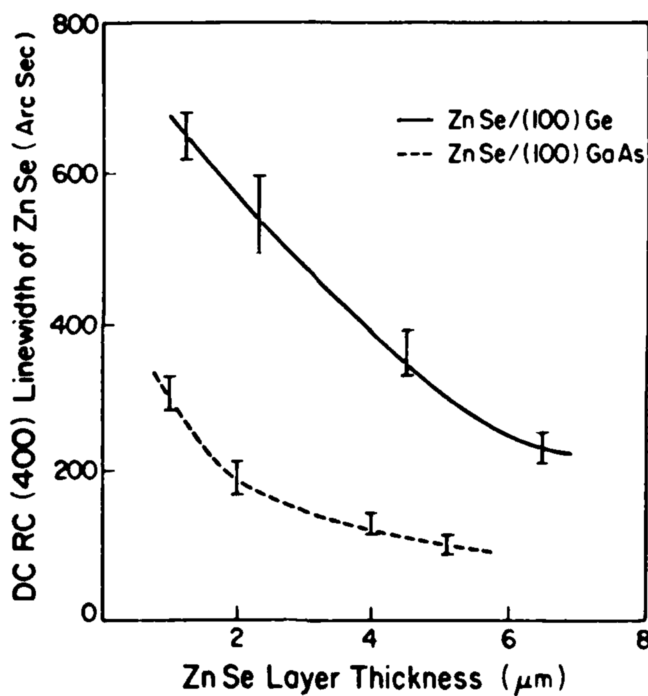

Figure 2-6. Double crystal rocking curve (DCRC) (400) linewidth data recorded from ZnSe/GaAs and ZnSe/Ge layers grown under a fixed set of growth conditions to various thicknesses.

As can be seen from the figure, both sets of data exhibit the commonly observed inverse relationship of DCRC linewidth to layer thickness. The bars drawn in Figure 2-6 are not error bars but, in fact, correspond to the range of DCRC linewidths recorded from each layer as a function of angular position of the sample with respect to the x-ray beam. Each sample is being rotated through a full 360° in the sample plane.

A rather surprising result indicated by the data plotted in Figure 2-6 is that, for any given layer thickness, the DCRC linewidths recorded from ZnSe/Ge layers are at least a factor of two larger than those from ZnSe/GaAs layers. This is despite ZnSe/Ge representing the smaller lattice-mismatched system. Clearly then, an additional structural phenomenon is responsible for the DCRC linewidth broadening in ZnSe/Ge layers.

In order to investigate the additional structural phenomenon suspected of reducing ZnSe/Ge layer quality, a detailed study was made of rocking curves recorded as a function of angular position of the sample for both ZnSe/Ge and ZnSe/GaAs layers. The study involved measuring the separation, D, between the layer and substrate (400) reflection peaks at various angular positions obtained by rotating the sample about its normal while keeping the x-ray beam position fixed.

The measured values of D, the angular separation between the layer and substrate reflection peaks, are plotted in Figure 2-7(a) for a typical ZnSe/GaAs sample as a function of rotation angle, α. As can be seen from the figure, D exhibits a cosinusoidal variation with α. In fact, D is composed of two contributing terms, $\Delta\Theta$, the lattice-mismatch (a constant) and $\Delta\phi\cos\alpha$, a tilt term; i.e., the ZnSe layer planes are tilted with respect to the GaAs substrate planes. The layer/substrate peak separation angle is given by

$$D = \Delta\Theta + \Delta\phi\cos\alpha$$

where $\Delta\Theta = 1/2\ (D_{max} + D_{min})$

and $\Delta\phi = 1/2\ (D_{max} - D_{min})$

where D_{max} and D_{min} are the measured maximum and minimum values of the angular separation between the layer and substrate reflection peaks.

The data obtained from the ZnSe/GaAs layer illustrated in Figure 2-7(a) yields a lattice-mismatch of ~ 0.26%; i.e., close to the bulk value, and a tilt angle of 40".

The cosinusoidal variation of D on account of tilt can be explained using a modified version of the model employed by Hattanda and Takeda which is illustrated in Figure 2-7(b). In the model, a cone representing the Bragg condition for the ZnSe layer is shown tilted with respect to the GaAs substrate Bragg cone.

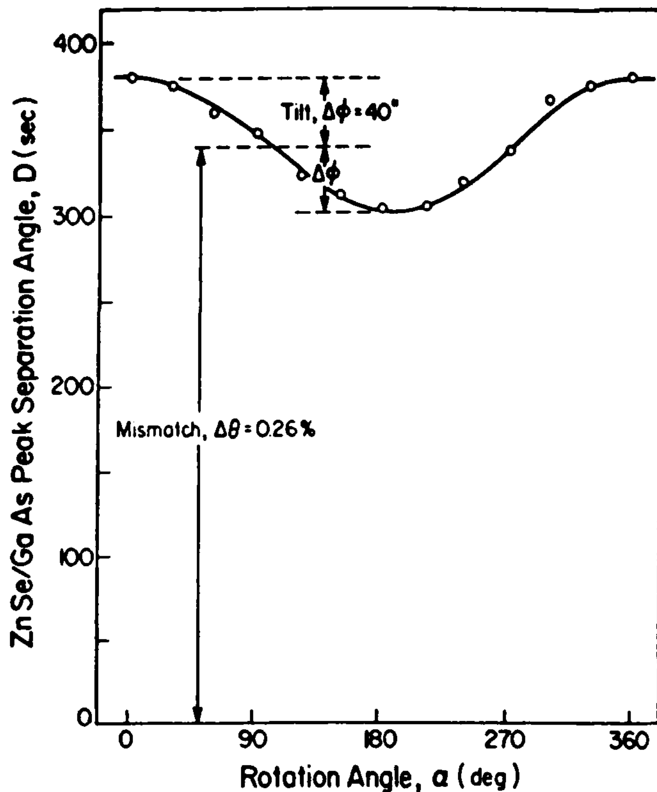

Figure 2-7(a). Layer/substrate model peak angular separation plotted as a function of rotation angle for a typical ZnSe/GaAs sample.

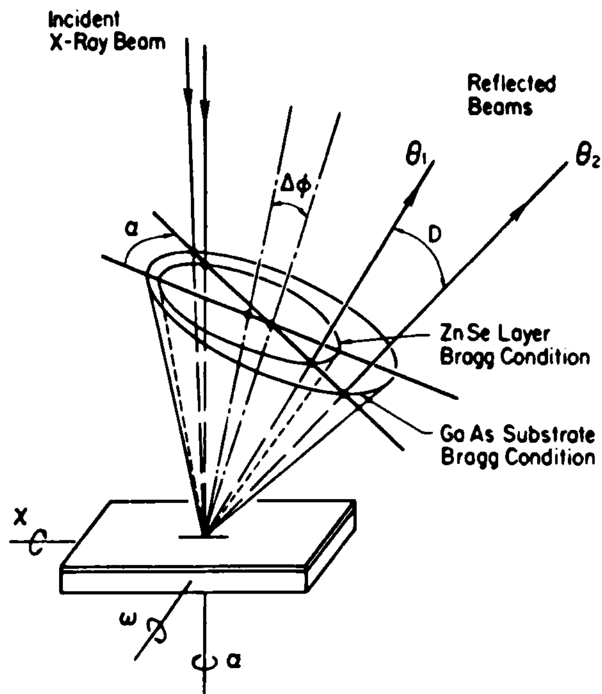

Figure 2-7(b). Bragg reflection for the ZnSe/GaAs sample.

As seen from the figure, rotation of the incident x-ray beam as indicated, which is equivalent to rotating the sample about its normal while keeping the x-ray beam fixed, will result in the angular separation of the detected layer and substrate reflected beams being a maximum for $\alpha = 0$, a minimum for $\alpha = 180°$, and a maximum again for $\alpha = 360°$. In all cases, the sample was rocked about the ω-axis and the intensity of the substrate reflected beam was maximized by adjustment about the χ-axis.

A similar sample rotation procedure carried out on a typical ZnSe/Ge layer provided the data shown in Figure 2-8(a). As can be seen from the figure, the tilt angle recorded; i.e., $\Delta\phi = 960"$, is very much larger than that determined for the ZnSe/GaAs layer discussed above, while the lattice mismatch, $\Delta\Theta$, is close to the bulk value at ~ 0.18%. Also notable regarding the data illustrated in Figure 2-8(a) is the fact that for certain values of rotation angle α, the measured peak separation angles have a negative sign.

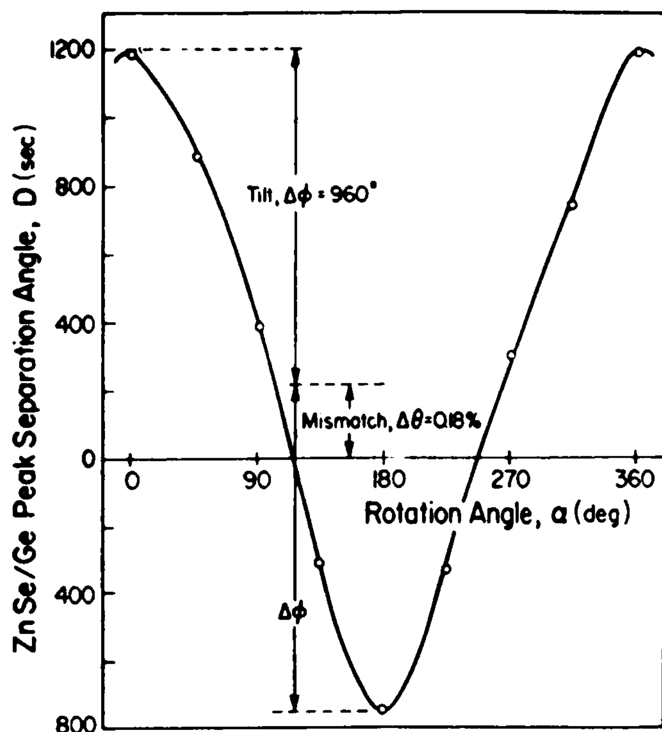

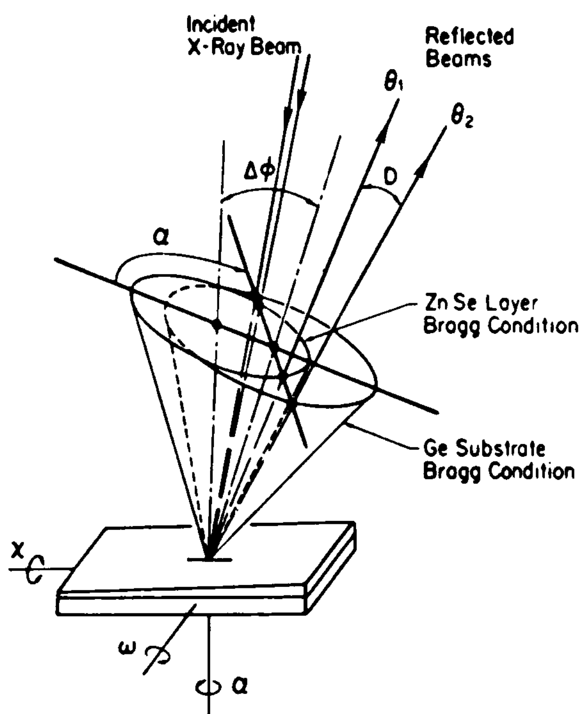

Figure 2-8(a). Layer/substrate model (400) peak angular separation plotted as a function of rotation angle for a typical ZnSe/Ge sample.

Figure 2-8(b). Bragg reflection for the ZnSe/Ge sample.

This observation can be explained with reference to the cone model shown in Figure 2-8(b). In this case, it is assumed that the tilt is so large that part of the base of the ZnSe layer cone lies outside the base of the Ge substrate cone. It can be seen from this case that indeed there will be a sign reversal of D on rotation of the sample about its normal.

The additional structural phenomenon reducing ZnSe/Ge layer quality then appears to be the large degree of tilting discussed above experienced by ZnSe/Ge layers relative to that exhibited by ZnSe/GaAs layers grown under the same conditions. It is suspected that dislocations form in the bulk of the ZnSe/Ge layers on account of the tilting, thus broadening the DCRC peak linewidths. However, the possibility that dislocations actually produce the tilting of the layers with respect to the substrate orientation cannot be ruled out.

2.1.2.2 Photoluminescence Analysis

In addition to the DCRC peak linewidths being recorded from the ZnSe/GaAs and ZnSe/Ge layers grown in the thickness range 1 μm to 6.5 μm, the DBE peak linewidths were also measured for this set of samples. The DBE linewidth data is illustrated in Figure 2-9. As can be seen from the figure, the DBE linewidths recorded from ZnSe/GaAs layers appear to be relatively insensitive to layer thickness variations over the range investigated, with linewidths measured remaining around 1 meV. On the other hand, the DBE linewidths recorded from ZnSe/Ge layers show a strong dependence on layer thickness, decreasing from over 3 meV for 1 μm thick layers to around 1.2 meV for 6.5 μm thick layers. Given that DBE linewidths are also broadened by lattice inhomogeneities associated with structural defects such as dislocations, the PL analysis seems to support the postulate discussed above. That is, that dislocations propagate in the bulk of the ZnSe/Ge layers probably on account of the relatively high degree of tilting experienced by these layers. Dislocations in ZnSe/GaAs layers would appear to be confined to the substrate/layer interface region.

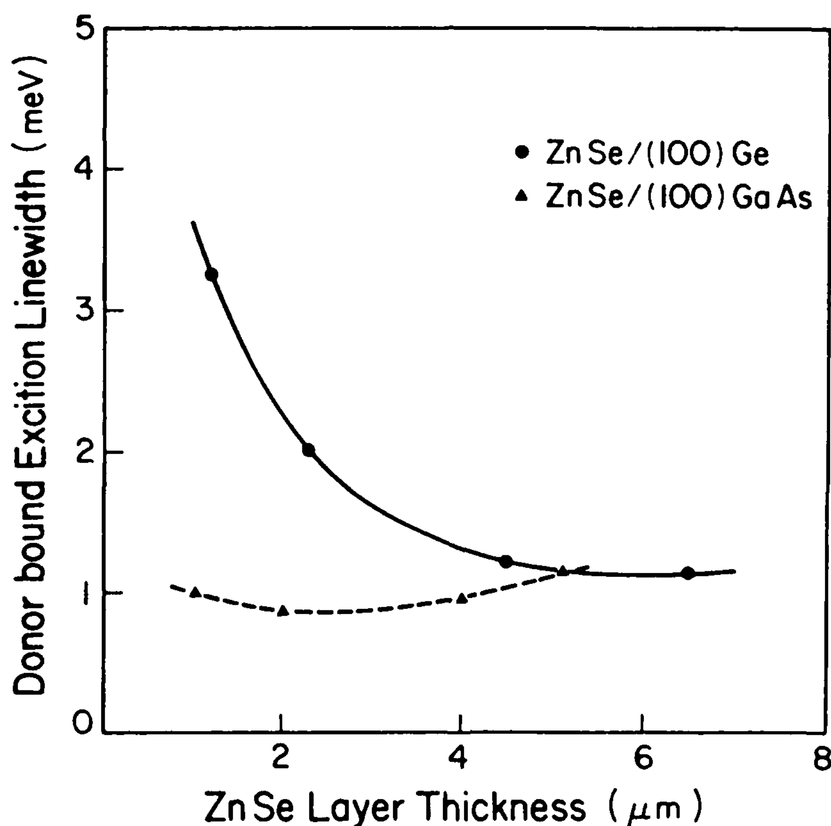

Figure 2-9. Donor-bound exciton (DBE) linewidth data obtained from 4.2K PL measurements of ZnSe/GaAs and ZnSe/Ge layers grown to various thicknesses under a fixed set of growth conditions.

The results of cross-sectional transmission electron microscopy analysis of 2 μm thick ZnSe/GaAs and ZnSe/Ge layers lend support to the above postulate. It was found that in the case of the ZnSe/Ge layer, dislocations are present in the bulk of the layer, whereas in the ZnSe/GaAs layer, the dislocation network is confined to the first 0.5 μm or so of material at the substrate layer interface. The results of cross-sectional and planar TEM will be discussed in Section 2.1.3.

2.1.3 Cross-Sectional and Planar Transmission Electron Microscopy: Defect Characterization of ZnSe/(100) Ge, ZnSe/(100) GaAs and ZnSe/(211) Ge

In this section, we will describe our initial observations on defects found in ZnSe grown on (100) GaAs and (100) Ge as well as (211) Ge, as observed by Conventional and Scanning Transmission Electron Microscopy. The specimens were thinned on an Ion Tech FAB 306 atom mill using Ar gas. The planar samples were dimpled and milled from the substrate side only. Atom milling was performed at an angle of 30° and at 6 kV. At the end of the milling process, the angle was reduced to 15° and the voltage reduced to 2 kV for one hour to remove the layers damaged by the more energetic atoms.

The TEM studies were carried out on a 200 kV Hitachi H-800 and 300 kV Phillips-430. The electron channeling patterns were taken on a JEOL-840 scanning electron microscope. The cross-sectional samples of (100) GaAs and (100) Ge were prepared with (110) surface normals. This is convenient since the (100) planes are cleavage planes. The (211) Ge samples were cut with a diamond saw and the orientations were defined in the microscope later. A variety of defects were found in the cross-sectional and planar samples. A feature common to all samples was the presence of a large number of small dislocation loops giving black and white contrast and mottled appearance to the film surface. It has been shown [1] that this kind of defect is produced by ion or atom milling with Ar gas and can be eliminated or, in the case of ZnSe, reduced substantially using iodine rather than argon. We also attribute this kind of defect to the milling procedure. Among other defects, microtwins were observed in large quantities which are about ~ 30 Å wide and ~ 140 Å long, as well as stacking faults and dislocations. The chosen geometry of cross-sectional samples [with (110) surface normals for (100) GaAs and (100) Ge] is helpful in revealing defects because two sets of (111) slip planes may be viewed edge on. Electron channeling analysis performed with ZnSe/(100) GaAs, ZnSe/(100) Ge, and ZnSe/(211) Ge confirmed the epitaxial orientations for all epilayers.

2.1.3.1 ZnSe/(211) Ge

Figure 2-10 shows cross-sectional (a) and planar (b) views of a ZnSe/(211) Ge sample grown at 300°C. The presence of numerous microtwins and stacking faults is evident. As can be seen from Figure 2-10(a), some of the defects lie in the (111) planes. The interface [Figure 2-10(a)] is irregular and the ZnSe layer in the vicinity of the interface is faulted.

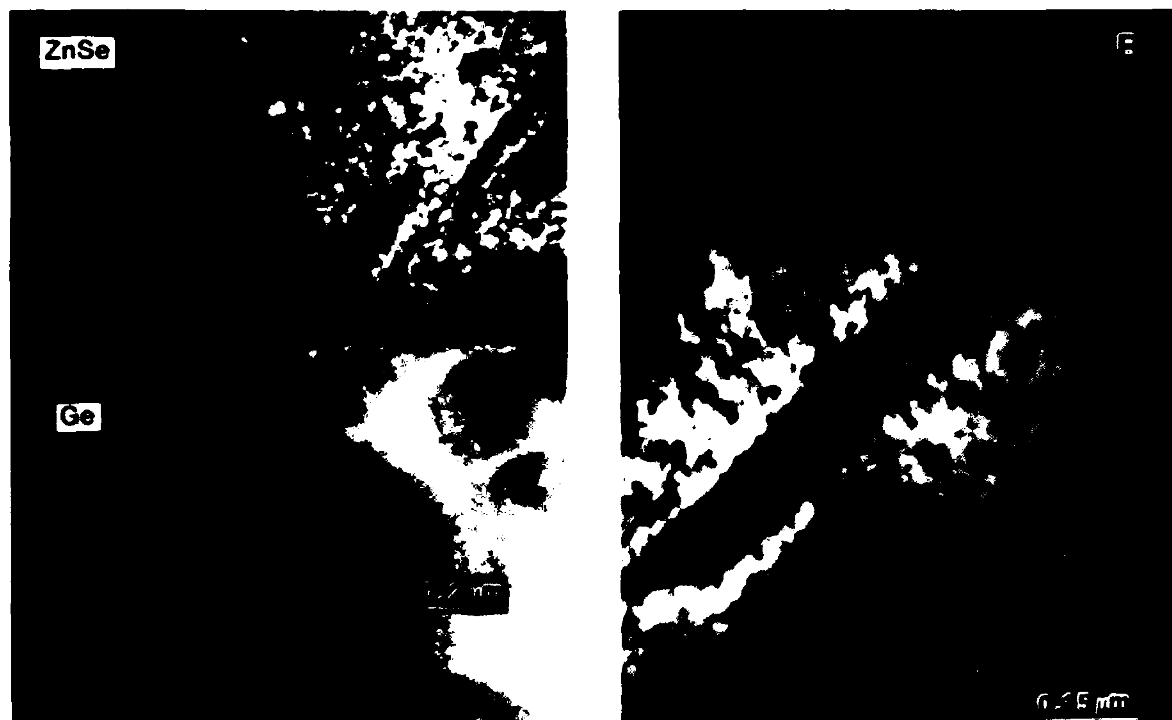

Figure 2-10. Transmission Electron Microscopy Images of ZnSe/(211) Ge Sample. (a) Cross-Sectional View, (b) Planar View

2.1.3.2 ZnSe/(100) Ge

Figure 2-11 illustrates cross-sectional (a) and planar (b) views of a ZnSe/(100) Ge sample grown at 330°C. As can be seen from Figure 2-11(b), the ZnSe/(100) Ge layer has what appears to be a dislocation cell structure. However, a more careful examination shows that these cell boundaries are, in fact, low angle grain boundaries. They exhibit very weak or no fringe contrast under a variety of bright field diffracting conditions. This suggests that the boundaries have extremely small rigid body displacements (much smaller than stacking faults, for example). The dislocations, in fact, reside within these boundaries accommodating any relaxation at the boundaries. It is interesting that very similar observations were recently made [2] on GaAs layers grown on (100) Si. This defect structure is

attributed to the later stages of growth of epitaxial layers which initially grow as islands with small misorientations between them [3]. Convergent Beam Electron Diffraction (CBED) analysis indicated that some of the boundaries are, in fact, anti-phase boundaries. It is interesting that the cell structure is not obvious in the cross-section [Figure 2-10(a)].

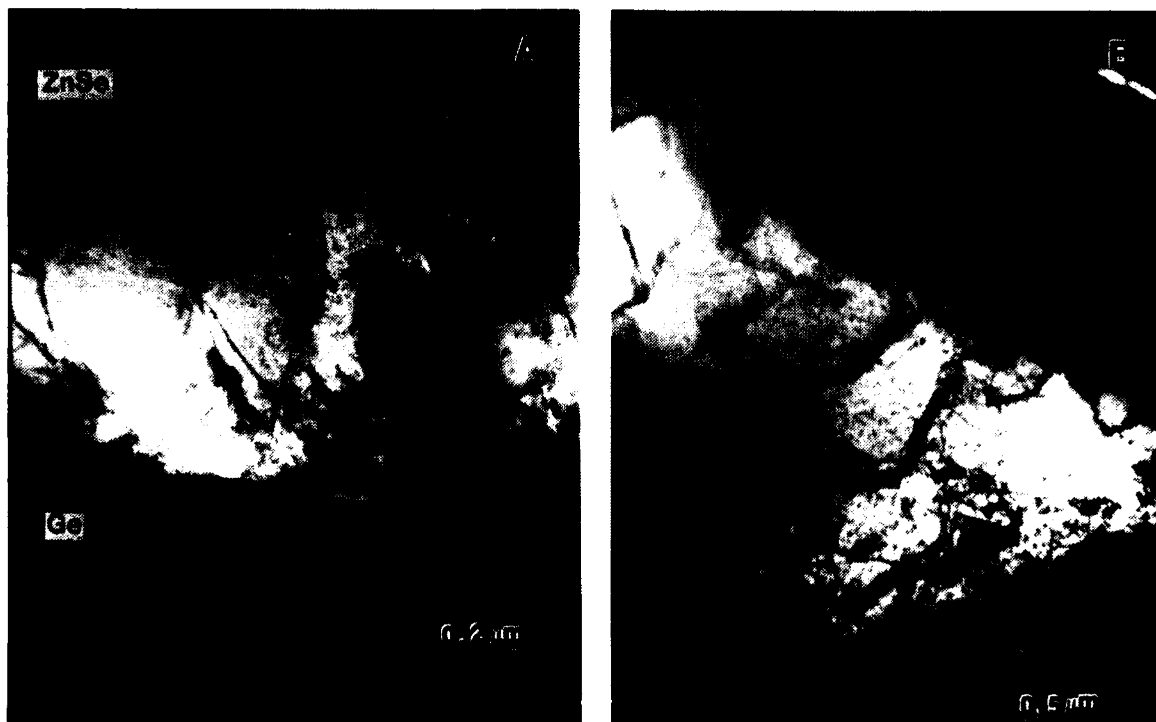

Figure 2-11. Transmission Electron Microscopy Images of ZnSe/ (100) Ge Sample. (a) Cross-Sectional View, (b) Planar View

However, a cross-section of a ZnSe/(100) Ge sample grown at 310°C exhibited a more pronounced grain structure. Microtwins were also found in the sample being evenly distributed throughout the bulk of the epilayer.

2.1.3.3 ZnSe/(100) GaAs

Figure 2-12(a) shows a cross-sectional view of a 1.5 μm thick ZnSe/(100) GaAs layer while a planar view of a 800 Å thick ZnSe(100) GaAs layer is shown in Figure 2-12(b). Both layers were grown at a substrate temperature of 330°C.

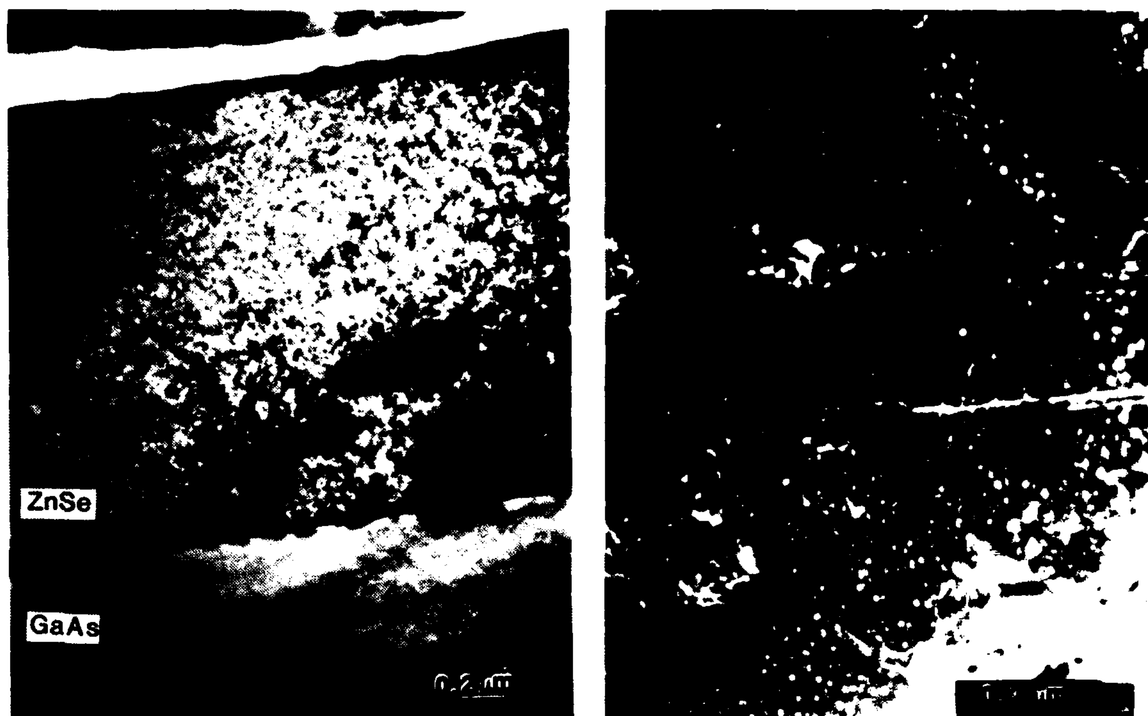

Figure 2-12. Transmission Electron Microscopy Images of ZnSe/(100) GaAs Sample. (a) Cross-Sectional View, (b) Planar View

Dislocations associated with the misfit between the substrate and the epilayer can be seen in Figure 2-12(b) as well as a network of dislocations not confined to the boundaries. The misfit dislocations could not be observed in other planar samples because of their thickness; however, in some cross-sectional samples at appropriate contrast conditions, dislocation induced strain fields could be observed [Figure 2-12(a)]. It was shown [4] that the strain field corresponds fairly well to the number of misfit dislocations introduced as a result of a mismatch of 0.26% between GaAs and ZnSe. As can also be seen from Figure 2-12(b), a close examination of Figure 2-12(a), which represents a sample grown to a thickness of ~ 1.5 μm does not reveal the stacking faults seen in the planar sample. Microtwins, on the other hand, were more obvious in cross-sectional samples than in the planar.

An examination of Figures 2-10(a), 2-11(a), and 2-12(a) indicates that the overall quality of ZnSe/(100) GaAs layers is superior to layers grown on (100) Ge and (211) Ge. These results are in good agreement with x-ray

double crystal rocking curve (DCRC) analysis and photoluminescence measurements (PL) performed up to date on ZnSe/(100) GaAs and ZnSe/(100) Ge samples.

Linewidths of the (400) reflection measured by the DCRC technique from ZnSe layers grown on (100) Ge are at least twice as large as those measured from layers grown under similar conditions on (100) GaAs [5]. It was also found in this study that the epilayers grown on (100) Ge are tilted up to 1000-1200 arc sec, with respect to the substrate, while the tilt for ZnSe on (100) GaAs was only 10-40 arc sec. It is not clear at the present time how the tilt affects the quality of ZnSe on (100) Ge, and what caused the tilt in the first place. We suspect however, that the surface geometry of the substrate obtained as a result of the cut-off angle used for (100) Ge and GaAs plays a very important role in the introduction of the tilt.

Photoluminescence analysis of the dominant donor-bound exciton (DBE) revealed that DBE linewidths recorded from ZnSe/GaAs layers are relatively insensitive to layer thickness variations (thickness $\geq$ 1 μm) while those from ZnSe/Ge layers show a strong dependence on layer thickness. These findings are in good agreement with the observations made in the present study, namely, that defects are present throughout the bulk of the ZnSe epilayers grown on (100) Ge, while being confined to a narrow interface region in ZnSe/(100) GaAs layers.

A comparison of ZnSe epilayer quality, evidenced by cross-sectional TEM analysis, as grown on (100) GaAs by MBE and MOCVD [6] suggests that MBE-grown layers are less faulted and have a smaller density of defects propagating through the layer to the free surface than MOCVD-grown layers. The results reported in this paper on TEM analysis of ZnSe/(100) GaAs layers can also be contrasted with those previously reported by Williams et. al. [7] which suggested the MBE-grown ZnSe layer examined in cross-section to contain a high concentration of microtwins propagating to the free surface. However, it should be noted that this layer was grown at a substrate temperature of 410°C compared with a substrate temperature of 330°C used in the present study.

ZnSe epilayers grown by MBE onto (100) GaAs, (100) Ge, and (211) Ge were examined in cross-sectional and planar TEM. A good correlation was found between the structural disorders revealed by TEM and the previous

x-ray and PL analyses. A striking difference was found between the ZnSe/(100) Ge and the other two orientations reported in this study, the ZnSe/(100) Ge exhibiting a cell structure.

2.2 Project 1, Task 2: Materials Research - p-ZnSe

Efforts to produce p-ZnSe by incorporation of acceptor impurities in high-purity ZnSe were increased substantially. We now are able to grow ZnSe unintentionally doped to a purity higher than before. There are strong efforts to dope ZnSe with Na as well as Sb, and perhaps to a lesser extent, P.

2.2.1 Na-Doped ZnSe on (100) GaAs

2.2.1.1 Na-Doped ZnSe: Growth and SIMS Characterization

It is quite puzzling to us that all the Na-doped samples are n-type in conductivity and their electron concentrations increase as the Na_2Se oven temperature increases. Low temperature PL spectra indicate the linewidth of I_x peak also increases with the Na_2Se oven temperature. It is likely that the increase in the electron concentration is due to either the increase of intrinsic defects because of increasing Na population on the growing surface or to the introduction of some unknown donor impurities. In order to find the real cause, Na_2Se was deposited on a clean Si substrate and the Na_2Se-coated Si substrate was examined in-situ by AES. It is found that the Na_2Se is contaminated with K (Figure 2-13) which is the major impurity in high purity Na metal. The role of K in ZnSe is unclear but it is not likely to be a donor. No other chemical species were found in the AES analysis; however, we have to keep in mind that the sensitivity of AES is about ~ 0.1% maximum. Other analysis techniques are necessary to detect impurities in lower concentrations.

Because of the difficulty in obtaining very high-purity Na_2Se source material for Na-doping, it was decided to do a SIMS survey of both doped and undoped samples. This was done in order to investigate the possibility of unintentional incorporation of donors from the dopant source.

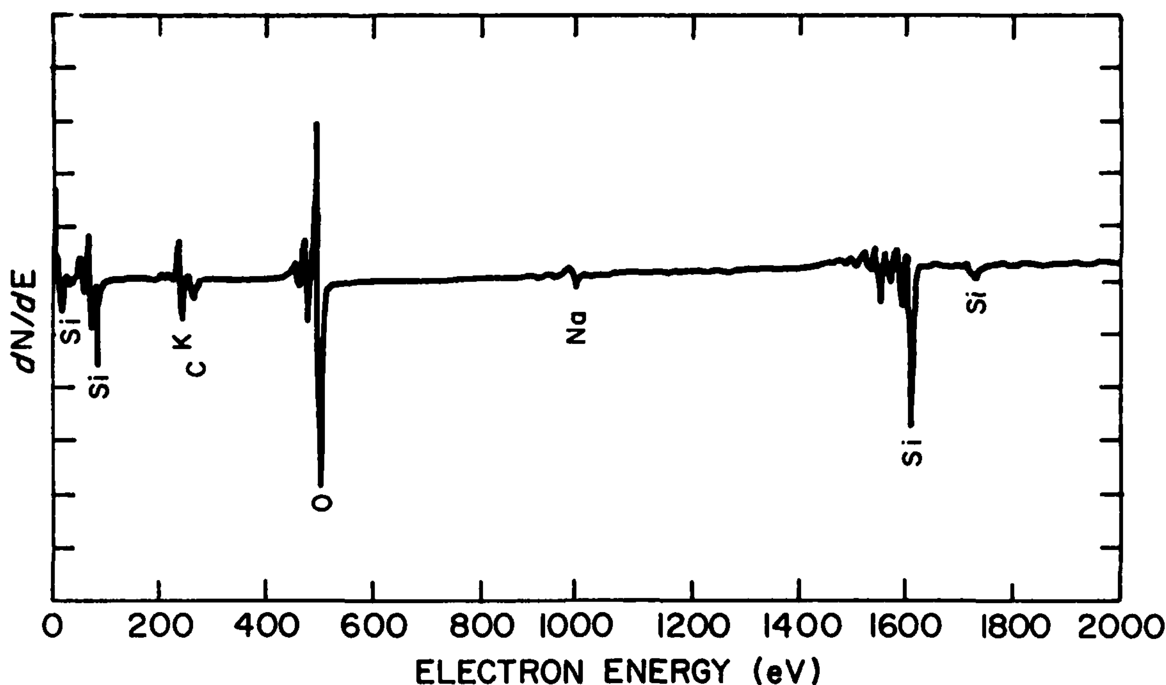

Figure 2-13. Auger spectrum of a Na-doped ZnSe/Si sample showing a prominent K peak.

Furthermore, such a study would assist in differentiating between donors resulting from impurities and those resulting from the creation of intrinsic defects due to the presence of the dopant flux.

The study was performed using both O_2^+ primaries with positive secondaries to detect electropositive species, and Cs^+ primaries with negative secondaries for electronegative species.

The O_2^+ analyses were carried out on the samples listed in Table 2-1. The undoped samples were chosen to represent a variety of starting materials. The Na and P doped samples were the most heavily doped available at the time. Data were taken in the mass spectrum mode, scanning through mass numbers 1 to 130. No Li, Be, or B were observed in the samples; other species of interest are tabulated in Table 2-2. The results of measurements of P-doped samples will be discussed in Section 2.2.3. ZSE73 was grown using Alfa (6N) Zn and Alfa (5N+) Se sources with Na_2Se as the source of dopant. SIMS analysis of this sample shows that it is heavily contaminated with K. Using an ion implanted calibration sample, the K concentration was found to be 1.9×10^{17} cm^{-3}. This is nearly equal to the Na concentration.

Apparently the K impurity is being selectively emitted by the Na_2Se source, or is being selectively incorporated in the ZnSe. This could be an important result, since the electrical behavior of K in ZnSe is unknown. The count rate for Al and Si was higher for all samples than the background count rate observed in earlier analysis. This is probably due to contamination of the SIMS system ("memory") from analysis of Si- and Al-containing photovoltaic structures. However, this has to be verified. Two more points of interest include the high Fe signal in ZSE93 and the high In signal in ZSE88. These observations may be attributed to the fact that ZSE93 was grown just as the Zn cell was running out, and ZSE88 was the first substrate to be In-soldered by a new laboratory person.

TABLE 2-1. Samples for O_2^+ SIMS Comparative Analyses.

Sample	Zn Source	Se Source	Dopant
ZSE26	Alfa (6N)	Spex (6N)	None
ZSE77	Alfa (6N)	Osaka Asahi (6N+)	None
ZSE88	Zone Refined	Osaka Asahi (6N+)	None
ZSE93	Zone Refined	Osaka Asahi (6N+)	None
ZSE94	Zone Refined	Osaka Asahi (6N+)	None
ZSE73	Alfa (6N)	Alfa (5N+)	Na_2Se
ZSE82	Alfa (6N)	Osaka Asahi (6N+)	Zn_3P_2

TABLE 2-2. SIMS Positive Secondary Ion Spectra.

(Counts/Second at $2x10^4$ Counts/Second ^{70}Zn)

Sample #

Element	Mass	26	77	88	93	94	73(Na)	82(P)
Na	23	50	300	10	100	50	2000	70
Mg	-	U	U	U	U	U	U	U
Al	27	100	50	10	400	200	200	80
Si	28	300	20	30	300	100	300	80
P	31	0	0	0	0	0	0	20
K	39	U	U	U	U	U	3000	U
Ca	44	4	0	0	3	4	4	3
Sc	45	0	0	0	0	0	0	0
Ti	48	10	0	0	30	20	4	8
V	51	0	0	0	2	0	0	0
Cr	52	5	2	0	7	5	0	U
Mn	55	2	0	U	6	0	0	0
Fe	56	20	2	U	100	20	2	7
Ni	58	4	20	0	5	3	2	4
Co	59	2	U	0	2	0	0	0
Cu	63	10	10	30	30	20	10	20
Ga	71	10	6	6	20	10	4	10
Ge	-	0	0	0	0	0	0	0
As	75	0	0	0	0	1	U	1
Pd	-	0	0	0	0	0	U	0
Ag	107	0	0	U	3	2	0	2
Cd	114	U	U	0	U	3	U	1
In	115	5	5	20	8	6	5	2
Sn	-	0	0	0	0	0	0	0
Sb	-	0	0	0	0	0	0	0

U = Spectrum obscured by other species, or peaks present but inconsistent with isotopic abundances.

The Cs^+ primary ion analyses for electronegative species were performed in two steps. First, the negative ion mass spectrum was scanned to find potential impurities (the negative spectra are much cleaner than positive spectra when voltage offset is used). Next, the impurity signals were quantified in the depth profile mode, using ion-implanted standards.

Table 2-3 presents the results of the Cs^+ analyses for As and Cu in the undoped and all Na doped samples, as well as some O_2^+ data for Na, Al, Ga, and In. The As and Cu background signals are believed to arise from actual As and Cu contamination in the implanted ZnSe epilayers.

TABLE 2-3. Depth Profile Analysis Results.
(in 10^{15} cm^{-3})

	n	[Na]	[As]	[Cu]	[Al]	[Ga]	[In]
			Na-doped				
68	20	4.5	240	110	-	-	-
69	210	6.3	310	150	-	-	-
70	290	4.5	190	73	-	-	-
72	120	10	190	73	-	-	-
73	180	200	72	50	40	5	1
			Undoped				
26	130	2	1200–6000	73	20	9	1
77	<0.10	2	130	44	10	5	1
88	<0.10	2	280	90	2	5	4
93	0.40	2	-	67	80	18	2
94	<0.10	2	95	130	40	9	1
Background	-	2	80	60	0.2	3	0.2

Both for As and for Cu, the level of contamination is large, and depending upon the behavior of the species, may have significant effects on sample properties. It is important to note that As, being non-metallic, is not considered in specifying the starting material purity. Cu, on the other hand, is considered; the $60\text{-}150\text{x}10^{15}$ cm^{-3} range reported here is in excess of the 6N ($\approx 22\text{x}10^{15}$ cm^{-3}) purity of the starting materials. This, of course, could result from differences in Zn and Cu sticking coefficients during film growth.

At present, the anamalously high As value for sample ZSE26 is not understood. This may have resulted from GaAs particulate contamination of the ZnSe films, from defects in the film, or from actual As contamination - possibly resulting from deviations in substrate preparation procedure.

Because of the high level of contamination present, it can be concluded that the doping behavior of Na was not actually tested in our work, and probably was not tested in work performed elsewhere (which used similar, or less pure, starting materials). Therefore, the first priority in the Na doping effort must be the development of means to introduce pure Na into the ZnSe films.

2.2.1.2 Na-Doped ZnSe: Photoluminescence

The main thrust of the St. Paul effort during the past quarter was in p-doping, using Na_2Se and Zn_3P_2. The PL measurements on all of these recently-grown films are summarized briefly in Table 2-4. In the case of Na-doping using Na_2Se, Table 2-4 indicates that, while the occurrence of donor-acceptor pair (DAP) emission in these samples indicates that acceptors are being incorporated at sizable levels, we observe a corresponding rise in the donor-bound exciton (DBE) emission.

This indicates that donors are being incorporated along with the acceptors. Note, for example, the monotonic increase of I_x with increasing Na_2Se cell temperature (samples ZSE68,69,70 or samples ZSE73,81). SIMS and Auger analyses of films grown using this Na_2Se indicate that this starting material is heavily contaminated and is, therefore, a likely source of undesirable donor atoms. In comparing samples ZSE76 (T_g=350°C, BPR=1/4:1) to ZSE72 (T_g=350°C, BPR=1:1) we find that higher BPR's favor the incorporation of acceptors over donors. This result was anticipated as a result of our earlier examination of the growth matrix for undoped material. Growth conditions near T_g=300-350°C, BPR=1/2:1-1:1 appear to be favorable for Na acceptor incorporation if a suitably "clean" source of Na can be obtained.

TABLE 2-4. Na_2Se Doping

$T(Na_2Se)$ = 450°C

BPR \ T_g	250°C	250°C	300°C	350°C
1/4:1				#76 I_x = 140,000 I_{DAP} = 680 I_{DL} = 340 R = 410
1/2:1	#71 I_x = 8,100 (I_1 = 3,300) I_{DAP} = 53,000 I_{DL} = 32 R = 253			#69 I_x = 110,000 I_{DAP} = 22,000 I_{DL} = 110 R = 1,000
1:1	#73 I_x = 7,400 (I_1 = 1,000) I_{DAP} = 310 I_{DL} = 110 R = 67	#87 (T_{Na}=400) I_x =320 I_{DAP} = 5 I_{DL} = 9 R = 36		#72 I_x = 100,000 I_{DAP} = 10,000 I_{DL} = 74 R = 1,350

T_g = 350°C, BPR = 1/2:1

BPR \ $T(Na_2Se)$	375	450	500
1/2:1	#68 I_x = 94,000 I_{DAP} = 56 I_{DL} = 22 R = 4,300	#69 I_x = 110,000 I_{DAP} = 22,000 I_{DL} = 110 R = 1,000	#70 I_x = 130,000 I_{DAP} = 16,000 I_{DL} = 360 R = 360

2.2.1.3 Na-Doped ZnSe: Electrical Characterization

The initial p-type doping attempts conducted at St. Paul involved the use of a Na_2Se cell as a source for Na. The parameters which were adjusted during this study included the temperature of the Na_2Se cell, the Zn:Se BPR, and the growth temperature. The effect of each was studied while holding the other two parameters constant. The results obtained from this investigation suggest that Na can be incorporated into ZnSe and that it forms a shallow acceptor level. Conversion to p-type conductivity during this study, however, was prevented by the incorporation of impurities which were present in the Na_2Se source.

The electrical properties the Na-doped films were found to depend strongly upon the temperature of the Na_2Se cell. The peak mobilities and room temperature carrier concentrations for samples grown at (BPR=1/2:1, T_g=350) with increasing Na_2Se cell temperature were measured to be:

SAMPLE	$T(Na_2Se)(°C)$	$n_{300}(cm^{-3})$	$\mu_p(cm^2/V\text{-}sec)$
ZSE67A	---	$2x10^{16}$	4000
ZSE68A	375	$2X10^{16}$	4000
ZSE69A	450	$2X10^{17}$	800
ZSE70A	500	$3X10^{17}$	600

These results were plotted in Figure 2-29 of Quarterly Technical Progress Report No. 3.

The concentration of carriers was found to increase and the peak mobility was found to decrease with increasing Na_2Se cell temperature. This type of behavior suggests that shallow donor levels are formed through one or more of the following mechanisms: (1) incorporation of Na on a undesirable site, (2) alteration of the growth kinetics due to the presence of Na_2Se which results in the formation of electrically active defects, and/or (3) contamination of the Na_2Se by some chemical species which is introduced into the film along with the Na. SIMS and PL measurements suggest that the last of these to be correct; the Na_2Se source is heavily contaminated and any attempts to dope with this source results in the incorporation of unwanted impurities.

The second study using the Na_2Se source investigated the effects of the Zn:Se BPR upon the incorporation of Na. The results of measurements made on samples which were grown with constant growth temperature, constant Na_2Se cell temperature, and variable BPR are shown in Figure 2-14. SIMS data also is included.

It can be seen that the electrical characteristics of the Na-doped films are only moderately dependent on the BPR. This suggests that in this region of growth parameter space, the incorporation of Na depends only weakly on the Zn:Se BPR.

The final study with the Na_2Se source investigated the effects of varying the growth temperature while holding the BPR and Na_2Se cell temperature constant. The results of this study are graphed in Figures 2-15(a) and (b) with the SIMS determinations of the Na concentration indicated. For both BPR=1/2:1 and BPR=1:1, the carrier concentration increased dramatically with increasing growth temperature. Since the room temperature carrier concentration is approximately equal to the difference between the donor and acceptor concentrations,

$$n_{300} \simeq N_D - N_A,$$

these results imply that either N_D increased or N_A decreased (or some combination of both) with increasing growth temperature. Surprisingly, the peak mobility increased along with the carrier concentration. The peak mobility roughly goes as the inverse of the sum of the ionized donor and acceptor concentrations,

$$\mu_P \sim (N_D^+ + N_A)^{-1}.$$

An increase in peak mobility, therefore, implies that $N_A^+ + N_D$ has been reduced. This suggests that the sum of the donor and acceptor concentrations in the samples discussed here should decrease with increasing growth temperature. In order to satisfy the demands set by the equations, we must conclude that the concentration of acceptors decreases much faster than the concentration of donors with increasing growth temperature. That is, N_A/N_D decreases with increasing growth temperature. Furthermore, if we assume the change in the carrier concentration is due only to the change in the acceptor concentration, then we find that the estimated change in the acceptor concentration agrees very well with the sodium content as determined by SIMS.

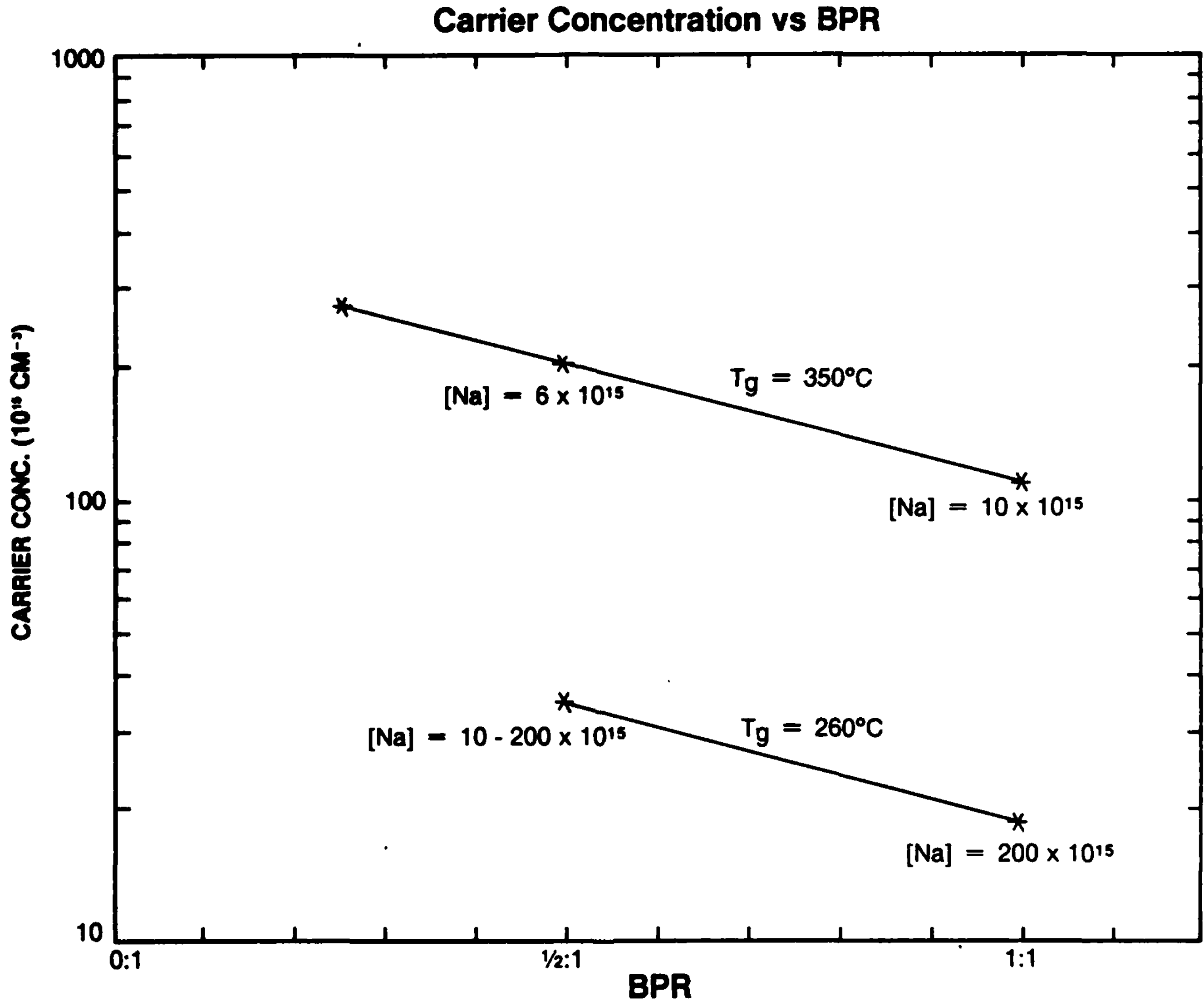

Figure 2-14. Carrier concentration plotted as a function of beam pressure ratio for two growth temperatures. Na concentrations determined by SIMS are indicated.

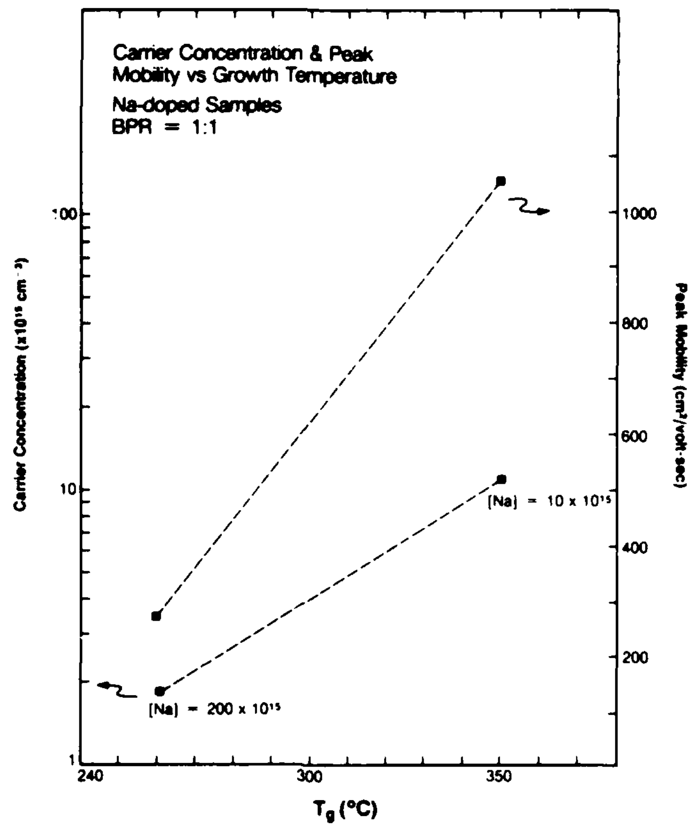

Figure 2-15(a). Carrier concentrations and peak mobilities for various growth temperatures with BPR 1:1.

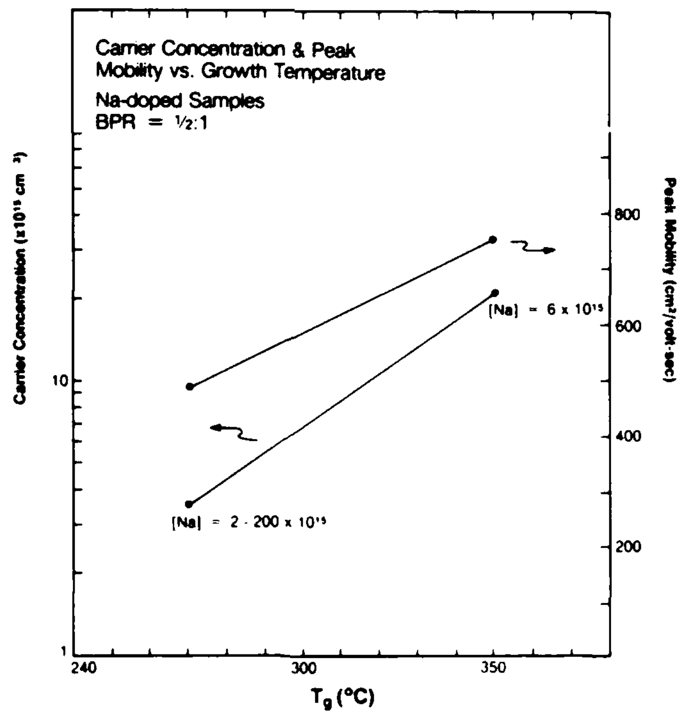

Figure 2-15(b). Carrier concentrations and peak mobilities for various growth temperatures with BPR 1/2:1.

The results obtained from the Na-doping study strongly suggest that Na forms a shallow acceptor level in ZnSe. Self-compensation does not appear to occur. Rather, impurities present in the dopant source inadvertently dope the sample n-type. This study indicates that if high purity Na_2Se were available, then p-type conversion in ZnSe could be accomplished.

2.2.2 Sb-Doped ZnSe on (100) GaAs

Sb doping was performed using the elemental 6N purity material effusing from a standard Knudsen cell. Sb is well behaved and does not require excessively high temperature for doping.

2.2.2.1 Sb-Doped ZnSe: Growth and SIMS Characterization

Antimony is a Group V element which, when it is a substitutional impurity on the Se site of the ZnSe lattice, has the potential to act as an acceptor impurity. Since, as far as we are aware, no work has been done in this area, and since Sb is a relatively well-behaved material, we decided to grow Sb-doped ZnSe.

In earlier work on N-doped ZnSe, the Zn/Se BPR was typically 10 since unintentionally doped ZnSe grown with this value of BPR exhibited a dominant free exciton PL spectrum. Such a spectrum suggests material of high purity. Recently, layers grown using 6N+ Se obtained from Osaka Asahi were found to exhibit a dominant free-exciton PL spectrum even for BPR's of unity. By way of contrast, earlier ZnSe layers grown using the Alfa chemicals supplied Se under similar growth temperatures and BPR exhibited a dominant DBE peak. This result suggests that donor impurities from the Alfa supplied Se were being incorporated in the ZnSe layers. It further suggests that the impurities belong to the Group III elements since their incorporation can be reduced by orders of magnitude (as determined by PL spectroscopy) simply by having and excess of Zn in the source fluxes.

What follows in this section, all results are for layers grown using the Osaka Asahi 6N+ Se source material, a growth temperature of 330°C, and a BPR=1.

Before using the Sb source it was found necessary to outgas the Sb at a monitored temperature of ~ 800°C. Prior to growth, the (100) GaAs substrate was sputter-cleaned and annealed. The Auger spectrum shown in Figure 2-16(a) reveals the absence of O and C. Growth was begun in the case of ZS-209 and ZS-210, with the Sb cell shutter closed. Half-order (2 x 1) surface reconstruction was observed for the first time (as far as we are aware) in the primary azimuth (110) during deposition of the undoped layers. This is shown in the RHEED pattern of Figure 2-17(a). It is noted that the reconstruction appeared after only a few seconds of growth. On subsequent opening of the Sb source shutter, the reconstruction intensified [Figure 2-17(b)] and the lines became sharper as seen in Figure 2-17(b). This is a rather amazing result which requires further study. Furthermore, an Auger spectrum taken of the Sb-doped ZnSe, ZS-209, after growth shows the presence of Sb. Because of the relatively low sensitivity of the AES technique, the result suggests Sb surface concentrations in excess of $10^{19} cm^{-3}$. The films, grown at the two highest Sb cell temperatures, namely 800°C monitored (ZS-209) and 700°C (ZS-210), were found to have a milky appearance suggesting rough surfaces. This was subsequently confirmed by scanning electron microscopy. There was no evidence of Sb in the Auger spectrum of ZS-210 grown using the lower Sb cell temperature.

In order to check the results, a series of layers (ZS-211 to ZS-214) were grown on (100) GaAs:Cr substrates. ZS-211 was undoped and ZS-212 to ZS-214 doped with the Sb cell at various temperatures. It should be noted here that after ZS-210 was grown, the Sb cell configuration was changed so that, even though the cell temperatures used for ZS-212 to ZS-214 were lower than that of ZS-209 and ZS-210, the fluxes are comparable. A SIMS analysis was performed using both a Cs^+ primary beam with negative secondary ion detection, and an O_2^+ beam with positive secondary ion detection. Although the Cs^+ beam provides an order of magnitude higher specific ion yield, because the samples were grown on insulating GaAs, charging problems prevented the use of high primary beam currents. Therefore, better sensitivity was achieved with the O_2^+ primary beam and positive secondaries, because the electron flood gun could be used to overcome charging effects. In this mode, detecting the $^{121}Sb^+$ ion with the $^{70}Zn^+$ ion for reference, and using an ion-implanted standard, a detection limit of about $5x10^{15}$ cm^{-3} was achieved.

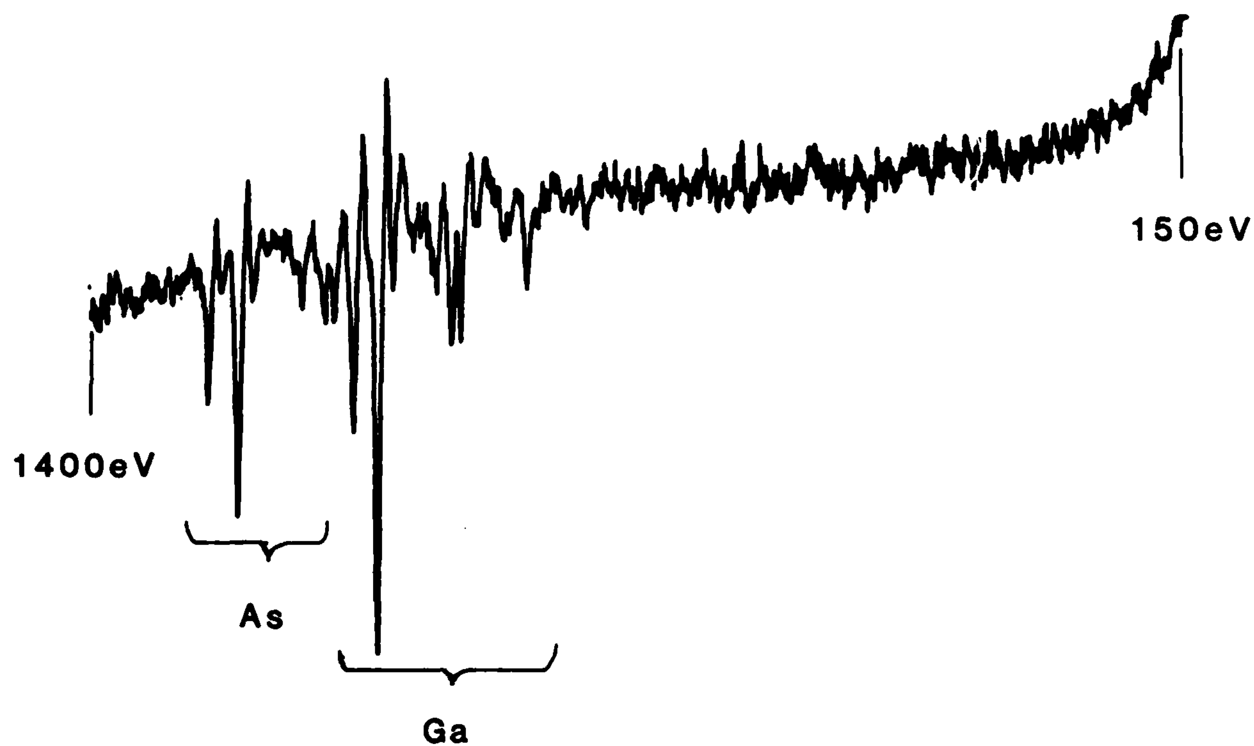

(a) Sputtered and annealed (100)GaAs

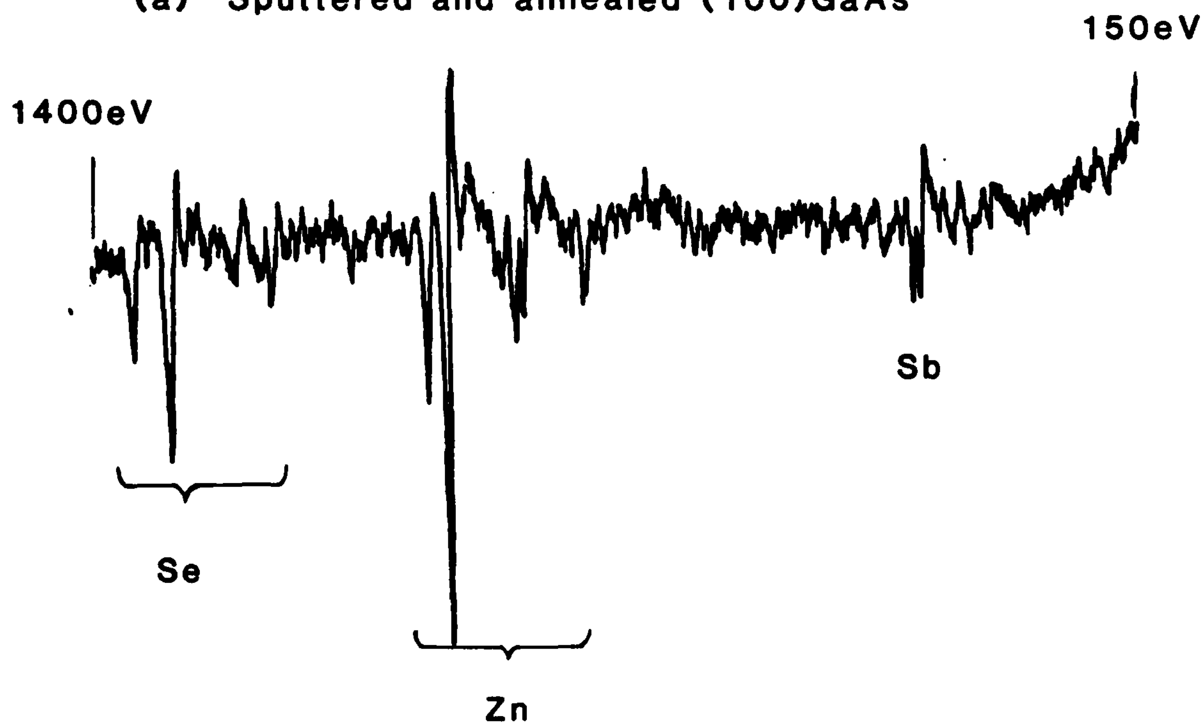

Figure 2-16. Auger spectra of (a) undoped and (b) Sb-doped ZnSe layers. Note the Sb peak is present indicating very high Sb surface concentrations.

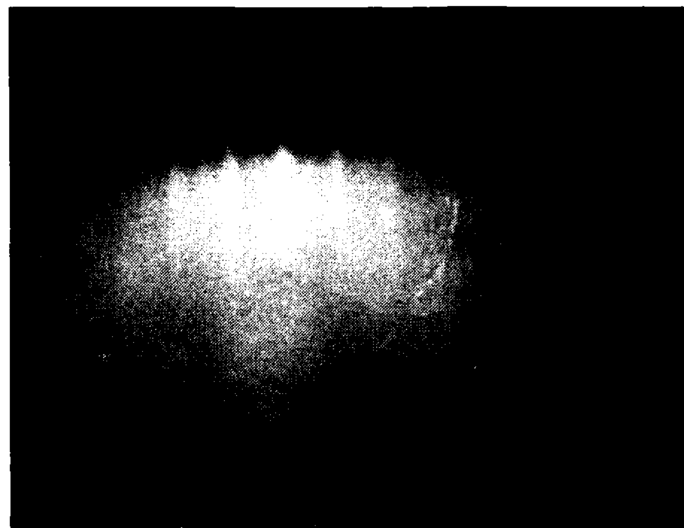

Undoped ZnSe

Layer

$[1\bar{1}0]$ azimuth

(a)

Following opening

of the Sb shutter

$[1\bar{1}0]$ azimuth

(b)

Figure 2-17. RHEED pattern of the undoped ZnSe along the $(1\bar{1}0)$ azimuth showing 1/2-order reconstruction. The pattern is intensified when the Sb-shutter is opened.

Results of depth profiling analyses on the Sb doped samples are presented in Table 2-5. Only one of the samples, #212, showed Sb incorporation significantly above the background. This sample also showed a surface enhancement of the Sb concentration of about 10 times the bulk value, persisting to a depth of about 0.07 micron below the surface. It should be noted that for samples with detectable Sb, concentration values obtained using Cs^+ and O_2^+ analysis modes agreed to within 30%.

TABLE 2-5. Sb Doping Parameters.

Sample #	Substrate Temperature (°C)	BPR	Sb Cell Temperature (°C)	[Sb] (10^{15} cm^{-3})
211	330	1	R.T.	< 4.8
212	330	1	600	73
213	330	1	550	5.8
214	330	1	500	< 4.8

2.2.2.2 Sb-Doped ZnSe: Photoluminescence

Low-temperature (4.2K) photoluminescence measurements were made of samples ZS-211 to ZS-214. These measurements did not provide conclusive evidence that Sb was being incorporated into the ZnSe in detectable concentrations. The 4.2K PL spectrum taken of ZS-211 (undoped layer) is shown in Figure 2-18(a). The spectrum is seen to be dominated by the free-exciton emission peak at about 2.8026 eV. The excitonic band is shown in detail in Figure 2-18(b) and three resolved peaks at 443.4 nm, 443.22 nm, and 443.32 nm, probably associated with donor levels, are observed. Figure 2-19(a) shows the 4.2K PL spectrum of ZS-212 which was the most heavily doped layer. A comparison of this spectrum with that of the undoped layer, ZS-211 [Figure 2-19(a)], shows that a prominent peak we have labeled I_1 at 445.4 nm, is now evident. This peak is seen in greater detail in Figure 2-19(b) with a LO-phonon replica also evident at 450.5 nm. At the lower Sb cell temperatures used for ZS-213 and ZS-214, the peaks at 445.4 nm could just barely be discerned. SIMS data of Table 2-5 indicates that the Sb concentration in the "bulk" of the layer is about 12 times greater in ZS-212 than ZS-213, and below the detection level for ZS-214.

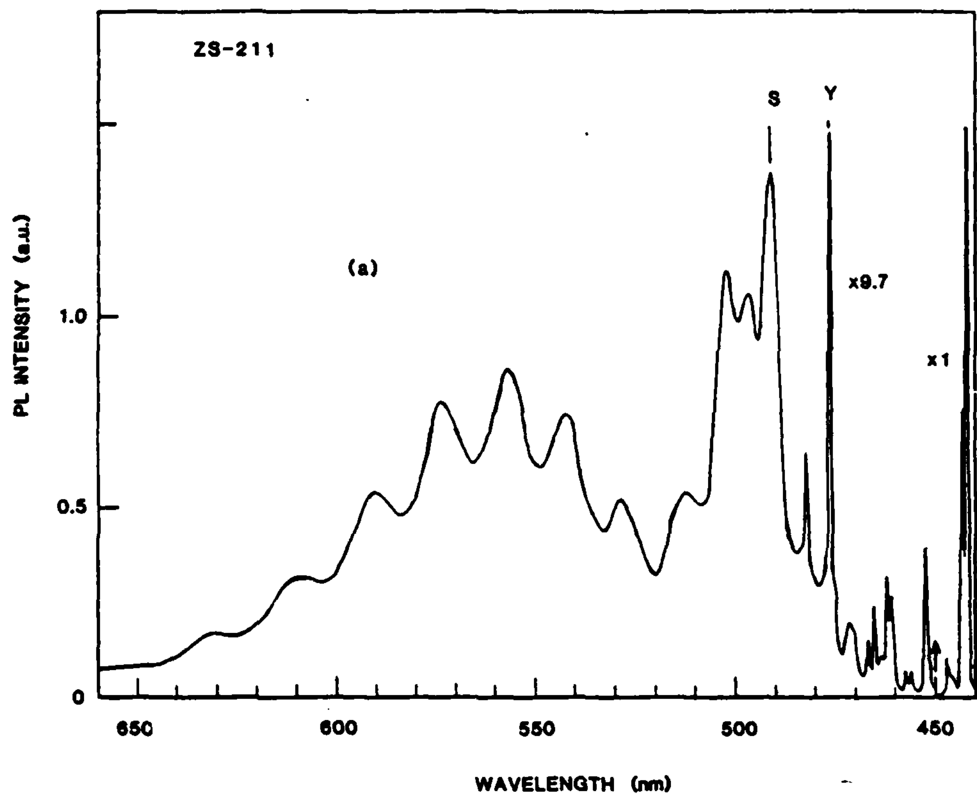

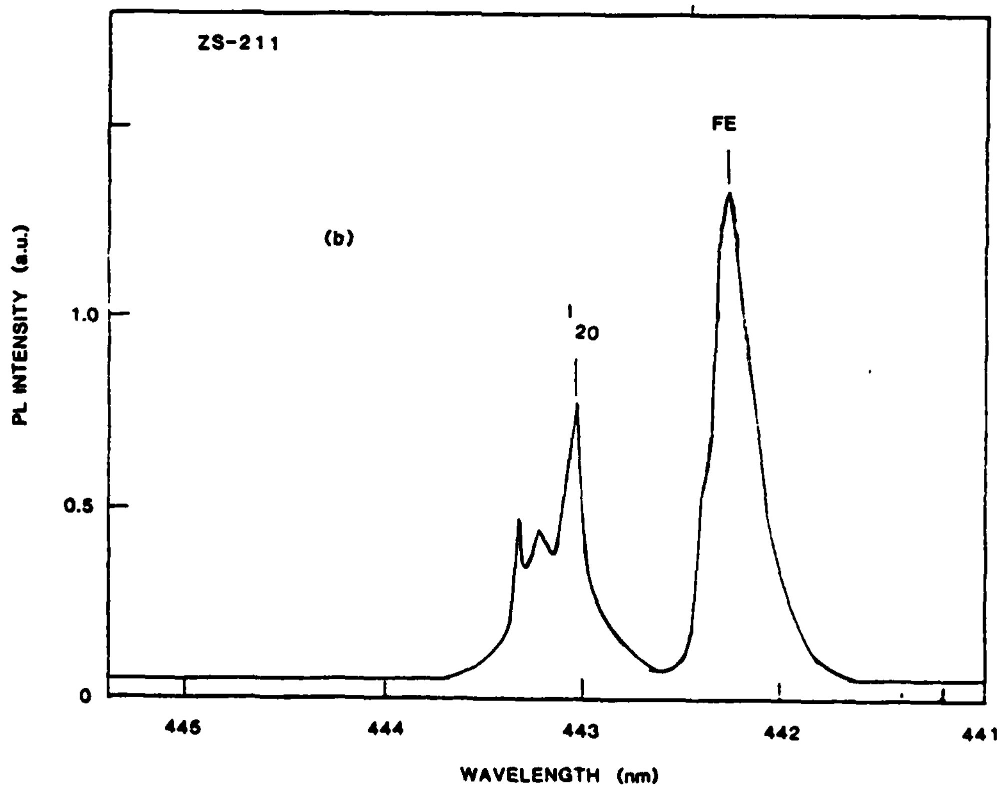

Figure 2-18. 4.2K PL spectrum of (a) undoped ZnSe/(100) GaAs grown using the 6N+Se source, and (b) shows the free exciton peak dominates the spectrum.

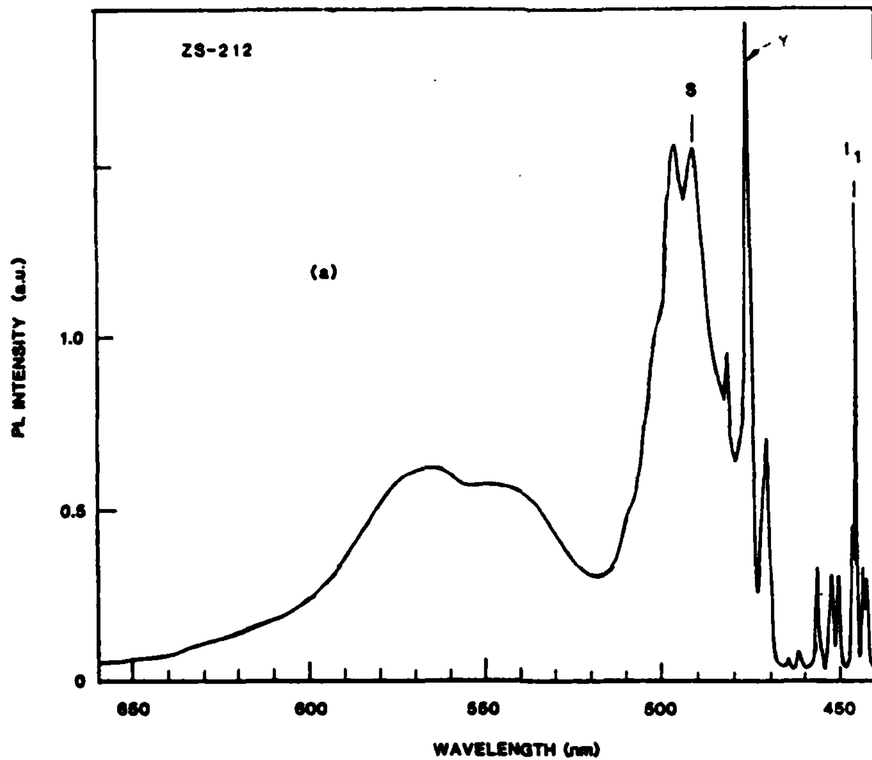

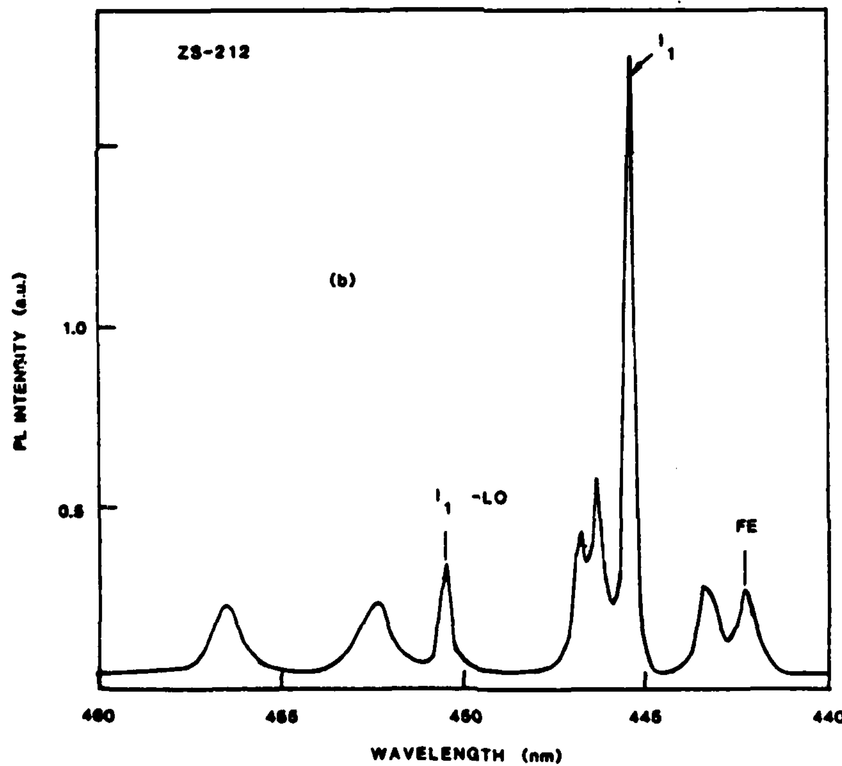

Figure 2-19. (a) 4.2K PL spectrum of the most heavily Sb-doped layer. The only significant new peak when compared with that of the undoped material is I_1 shown in greater detail in (b). However, I_1 may be I_1^{deep} associated with Cu and/or defects.

Although it is tempting to attribute this peak (445.4 nm) to Sb substitutional impurities, we should caution that in earlier undoped samples - especially ZnSe grown on (100) Ge - a relatively strong peak was observed at about the same wavelength. We associated this with the so-called I_1^{deep} peak at 2.783 eV, commonly attributed in the literature to Cu and/or defects. Although the possibility exists, therefore, that the peak is due to substitutional Sb, it is equally likely that the introduction of high concentrations of Sb enhances the creation of a defect possibly associated with I_1^{deep}.

We should point out that relatively high Sb fluxes were required to obtain the I_1 peak. Indeed, the Auger spectrum taken of ZS-212 after completion of growth indicated the presence of Sb, and suggests surface concentrations in excess of $10^{19}/cm^{-3}$. However, SIMS analysis indicates "bulk" Sb concentrations of only ~ $7x10^{16} cm^{-3}$. These results suggest that although the sticking coefficient of Sb on ZnSe is high, the incorporation is relatively low. The relatively low incorporation or solid-solubility of Sb in ZnSe is not unreasonable seeing that the covalent radius of Sb (1.36 Å) is significantly larger than that of Se (1.14 Å) which it replaces in the ZnSe lattice.

2.2.2.3 Sb-Doped ZnSe: Electrical Measurements

An attempt was made to obtain electrical data on the Sb-doped samples ZS-212 to ZS-214. However, it was difficult to obtain ohmic contacts. As mentioned above, the surface was rough as determined by scanning electron microscopy and by the milky appearance. This is probably due to the very high concentrations of Sb on the layer surface and may well mean it is not possible to obtain electrical data. However, attempts will be made to anneal the contacts and failing this, then possibly etch back the top 0.1 - 0.2 μm of ZnSe.

2.2.3 P-Doped ZnSe on (100) GaAs

The first phosphorous-doping experiments at the St. Paul Laboratory made use of the compound Zn_3P_2 with 4N purity as the source of P.

2.2.3.1 P-Doped ZnSe: Growth

Thirteen P-doped ZnSe samples were grown under various conditions. The details of growth condition will be shown with either PL or Hall results. The phosphorus source used is Zn_3P_2 of 4N purity. Similar AES analysis was performed to check whether there are any major contaminants. The AES spectrum of Zn_3P_2-coated Si substrate shows that only Zn and P are present in addition to O and a small C peak. See Figure 2-20.

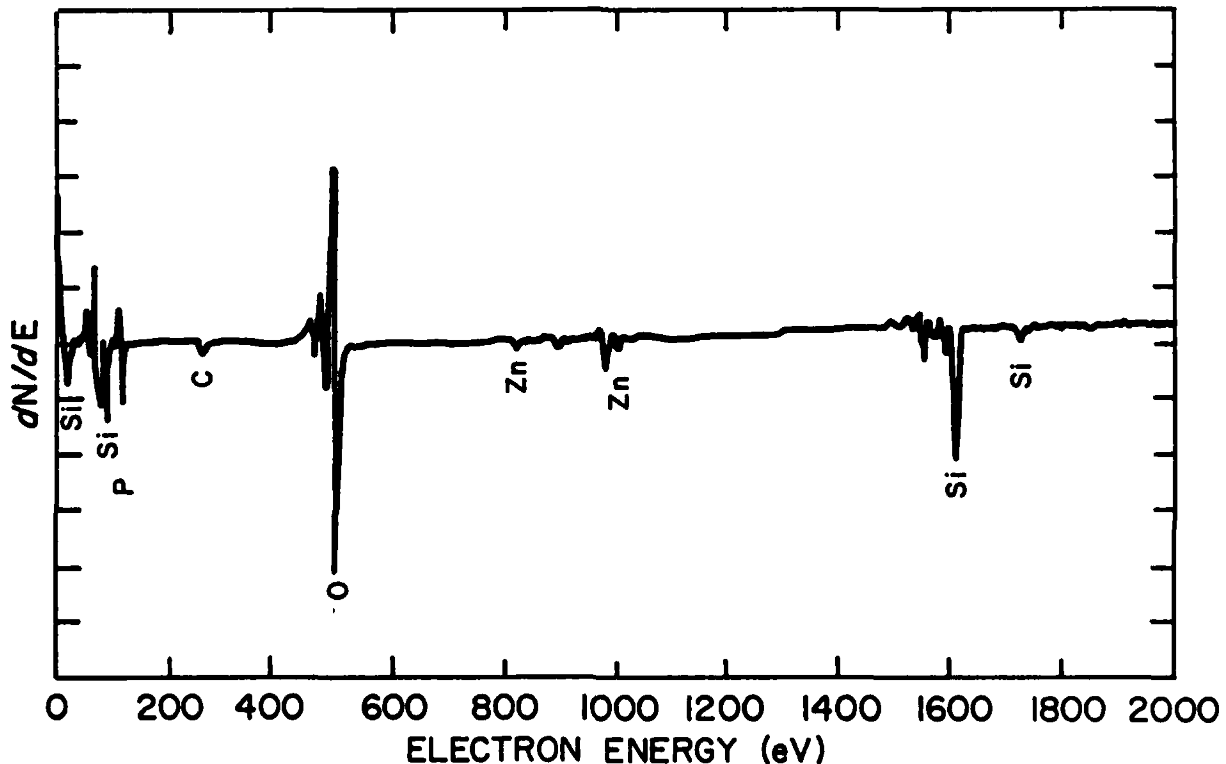

Figure 2-20. Auger spectrum of Zn_3P_2-coated Si substrate.

The doping studies consisted of two sets of experiments. In the first, the ZnSe growth parameters were kept constant, namely a substrate temperature of 350°C and a BPR of 1/2:1, while the Zn_3P_2 oven temperature was varied to produce different P fluxes. In the second, the Zn_3P_2 oven temperature was held constant at 500°C while the growth conditions were varied to study the relationship between growth conditions and P incorporation. The results of PL, Hall, and SIMS measurements will be discussed below.

2.2.3.2 P-Doped ZnSe: Photoluminescence

In our study of phosphorous doping from a Zn_3P_2 source (Tables 2-6 and 2-7), we find an increase in I_x as $T(Zn_3P_2)$ increases. (Compare samples ZSE78, 79, and 80.) In this case nothing much seems to come out of the Zn_3P_2 source until the cell temperature exceeds 400°C. Note, also, that the incorporation of donors in this sequence of samples is clearly not a "self-compensation" effect. In going from $T(Zn_3P_2)$=400°C (ZSE79) to 500°C (ZSE80), the increase in the number of acceptors (as measured by I_{DAP}, I_1, and, possibly, I_{DL}) is much smaller than the increase in the number of donors (measured by I_x). The increased donor concentration must be due to extrinsic donors from contaminated source material rather than to intrinsic defects accompanying the incorporation of acceptor atoms.

A more fundamental problem arises in these phosphorous-doping studies. In going from sample ZSE84 (T_g=350°C, BPR=1:1) to ZSE82 (T_g=250°C, BPR=1:1), we see a dramatic rise in the deep level emission relative to the near-band-edge emission intensity.

While the I_x intensity decreases from $2.7x10^4$ c/s to $3.5x10^3$ c/s, perhaps reflecting greater surface recombination because of degraded surface morphology, the DL emission actually rises by 10X. This effect is seen most clearly when comparing the actual PL scans, Figure 2-21. It would appear that small amounts of P can be incorporated as shallow acceptors but that, as the P-concentration increases, the P atoms complex to form deep levels. Such a possibility has been suggested previously [8]. The samples grown at $T(Zn_3P_2)$=450°C, Table 2-7, show that very little P or contaminant donor is emitted from the Zn_3P_2 cell at this temperature. The source cell temperature will have to be greater than or equal to 500°C for effective doping. Note that in samples ZSE898, 90, and 91 we see again the preferential incorporation of acceptors over donors as we move toward the Se-stabilized region (smaller BPR).

TABLE 2-6. Zn_3P_2 Doping

T(Zn_3P_2) = 500°C

BPR \ T_g	250°C	300°C	350°C
1/4:1			#85 I_x = 19,000 I_{DAP} = 1,020 I_{DL} = 60 I_{FE} = 5,400 R = 280
1/2:1			#80 I_x = 26,000 I_{DAP} = 3,200 I_{DL} = 280 I_{FE} = 4,600 R = 93
1:1	#82 I_x = 3,500 ($I_2 > I_x$) I_{DAP} = 27 I_{DL} = 390 I_{FE} = 1,400 R = 9	#83 I_x = 29,000 I_{DAP} = 230 I_{DL} = 66 I_{FE} = 4,400 R = 440	#84 I_x = 27,000 I_{DAP} = 520 I_{DL} = 33 I_{FE} = 4,800 R = 820
2:1			#86 I_x = 6,400 (I_1 = 830) I_{DAP} = 640 I_{DL} = 350 I_{FE} = 1,070 R = 18

TABLE 2-6. (Cont.)

T_g = 350°C

BPR \ $T(Zn_3P_2)$	300°C	400°C	500°C
1/2:1	#78 I_x = 2,100 I_{DAP} = 13 I_{DL} = 99 I_{FE} = 5,500 R = 21	#79 I_x = 2,000 I_{DAP} = 420 I_{DL} = 96 I_{FE} = 5,600 R = 21	#80 I_x = 26,000 I_{DAP} = 3,200 I_{DL} = 280 I_{FE} = 4,600 R = 93

TABLE 2-7. Zn_3P_2 Doping

$T(Zn_3P_2)$ = 450°C

BPR \ T_g	250°C	300°C
1/2:1	#89 I_x = 80 I_{DAP} = 110 I_{DL} = 11 I_{FE} = 120 R = 11	
1:1	#90 I_x = 750 I_{DAP} = 23 I_{DL} = 30 I_{FE} = 610 R = 25	
2:1	#91 I_x = 670 I_{DAP} = 12 I_{DL} = 18 I_{FE} = 312 R = 39	#92 I_x = 1,600 I_{DAP} = 5 I_{DL} = 13 I_{FE} = 690 R = 120

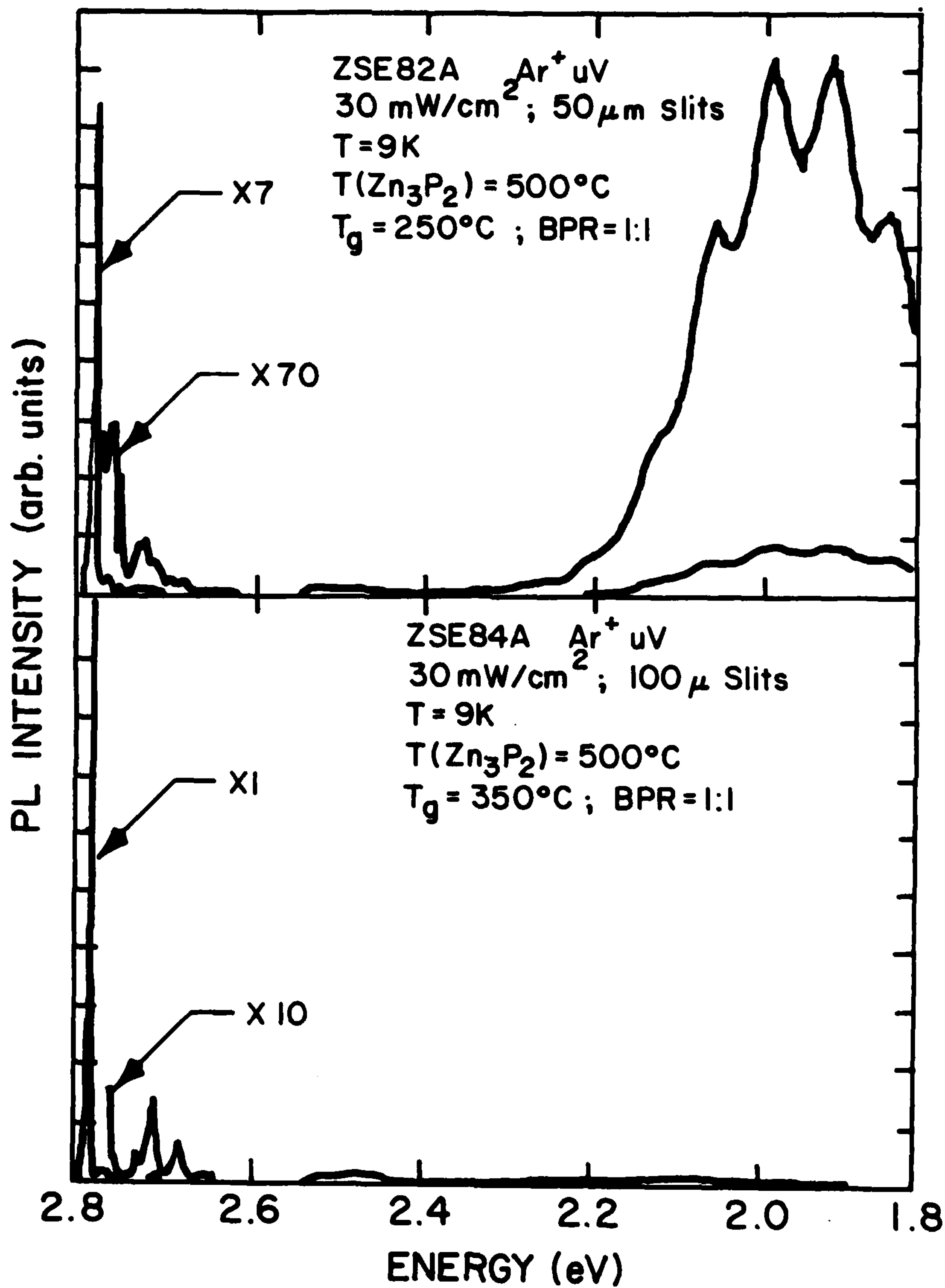

Figure 2-21. 9K PL spectra showing a dramatic increase in the deep level emission in changing T_g from 350°C to 250°C.

2.2.3.3 P-Doped ZnSe: SIMS Characterization

The P concentration in doped samples was determined from the $^{31}P^+$ secondary ion current generated by an O_2^+ primary ion beam, with the $^{70}Zn^+$ ion used as a reference signal. A P- ion-implanted ZnSe epilayer was used as a calibrated reference. Data were obtained in the depth profiling mode, and the detection limit, due to counting statistics, was about $1x10^{15}$ cm^{-3}. Results of the analyses are presented in Table 2-8 and in Figure 2-22. As in the Na doping work, substrate temperature is a dominant factor, and BPR a minor one, in controlling dopant incorporation. However, in the case of P, the dopant oven temperature seems more important than for Na, at least within the temperature ranges considered. In order to test the importance of thermally induced desorption of surface P on the bulk concentration, the logarithm of the P concentration was plotted versus the reciprocal temperature in Figure 2-22. The data do not strongly support this mechanism.

In order to test for the possibility of unintentional donor dopants being incorporated from the Zn_3P_2 source, the room-temperature electron concentration was plotted versus the Zn_3P_2 oven temperature in Figure 2-23; P concentrations are also included. Note that under these growth conditions (T_g = 350°C, BPR = 1/2:1), the P concentration is near the detection limit until the Zn_3P_2 cell temperature reaches 500°C. At this point the P concentration rises, and is accompanied by an abrupt increase in the electron concentration. Since the P concentration in this case is similar to that of the electron concentration, it is not clear whether an unintentional donor is being incorporated with the P, or the P itself is acting as a donor.

To test for possible unintentional donors, positive-secondary-ion SIMS spectra, analogous to those done for Na-doped samples, were performed (see Table 2-2). The spectra revealed no contamination levels beyond those of undoped samples. Negative secondary ion analyses of the P-doped samples have not yet been performed.

TABLE 2-8. P Doping Parameters

Sample #	Substrate Temperature (°C)	BPR	Zn_3P_2 Oven Temperature (°C)	[P]($x10^{15} cm^{-3}$)	$[n]_{300}$($x10^{15} cm^{-3}$)
ZSE78	350	1/2:1	300	1.0	$<10^{14}$
ZSE79	350	1/2:1	400	2.4	$<10^{14}$
ZSE80	350	1/2:1	500	5.0	$1.2x10^{16}$
ZSE82	250	1:1	500	90	$<<10^{14}$
ZSE83	300	1:1	500	9.0	$1.1x10^{15}$
ZSE84	350	1:1	500	3.0	$4.7x10^{15}$
ZSE85	350	1/4:1	500	2.8	$2.6x10^{15}$
ZSE86	350	2:1	500	3.0	$<10^{14}$
ZSE89	250	1/2:1	450	3.0	$<10^{14}$
ZSE90	250	1:1	450	3.4	$<10^{14}$
ZSE91	250	2:1	450	4-40*	$<10^{14}$
ZSE92	300	2:1	450	5	$2.3x10^{15}$
ZSE96	300	1:1	550	180	?

* non-uniform

2.2.3.4 P-Doped ZnSe: Electrical Characterization

Four films, ZSE77A-ZSE80A, were grown at (BPR=1/2:1,T_g=350) with ZnP cell temperatures of 20, 300, 400, and 500°C. The resistivity of the first three samples increased slightly with increasing ZnP cell temperature. The resistivity of ZSE80A, however, was much lower and the carrier concentration was measured to be $1x10^{16}$ cm^{-3}. Judging from the large mobility measured in ZSE80A (5000 cm^2/V-sec), we do not believe the ionized impurity or deep level concentrations to be too large. Therefore, the electrical measurements indicate the concentration of P is not large. This is consistent with the SIMS values shown in Table 2-8.

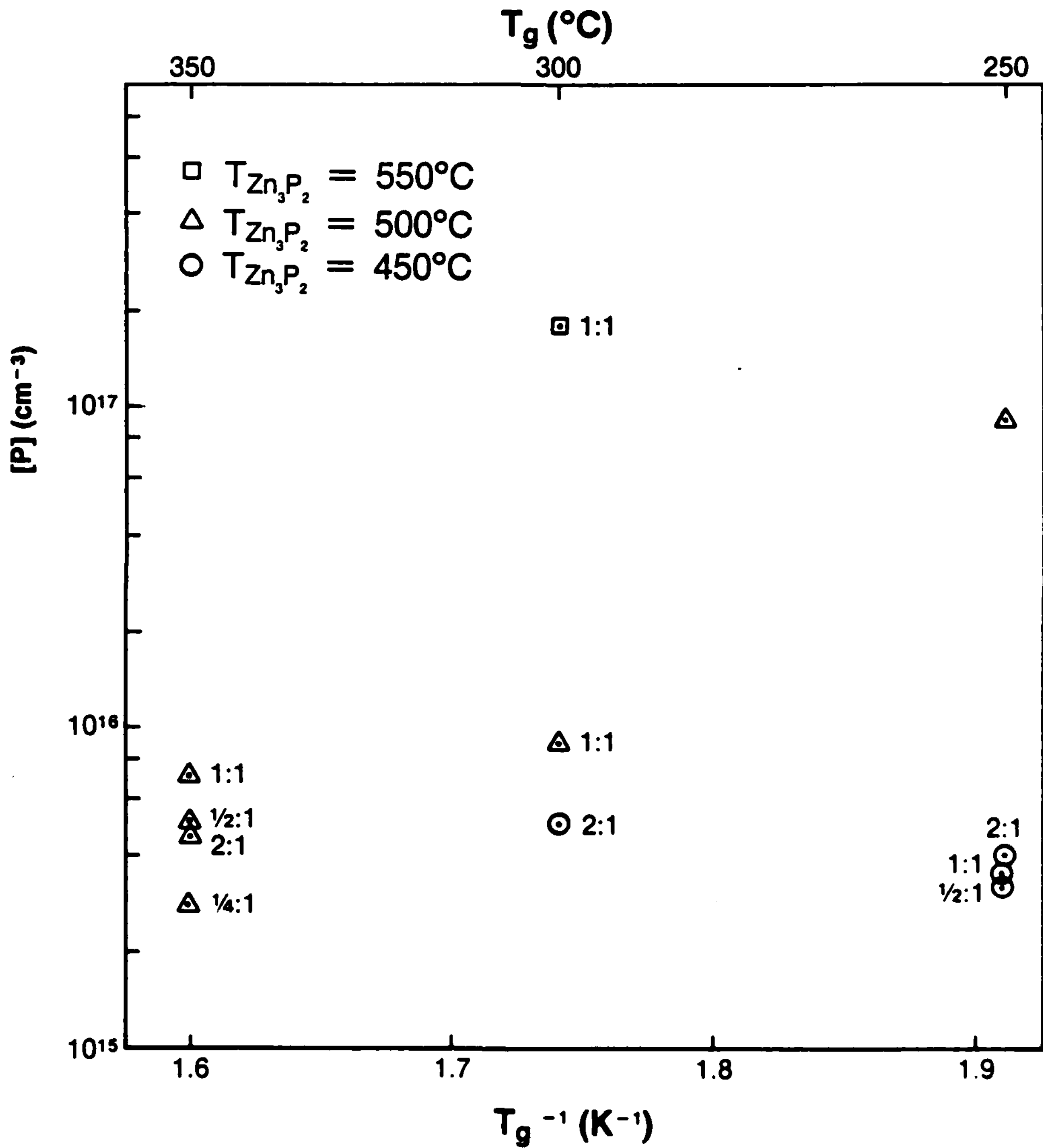

Figure 2-22. Plot of the P concentration versus the reciprocal growth temperature suggests that thermal desorption of surface P is not important.

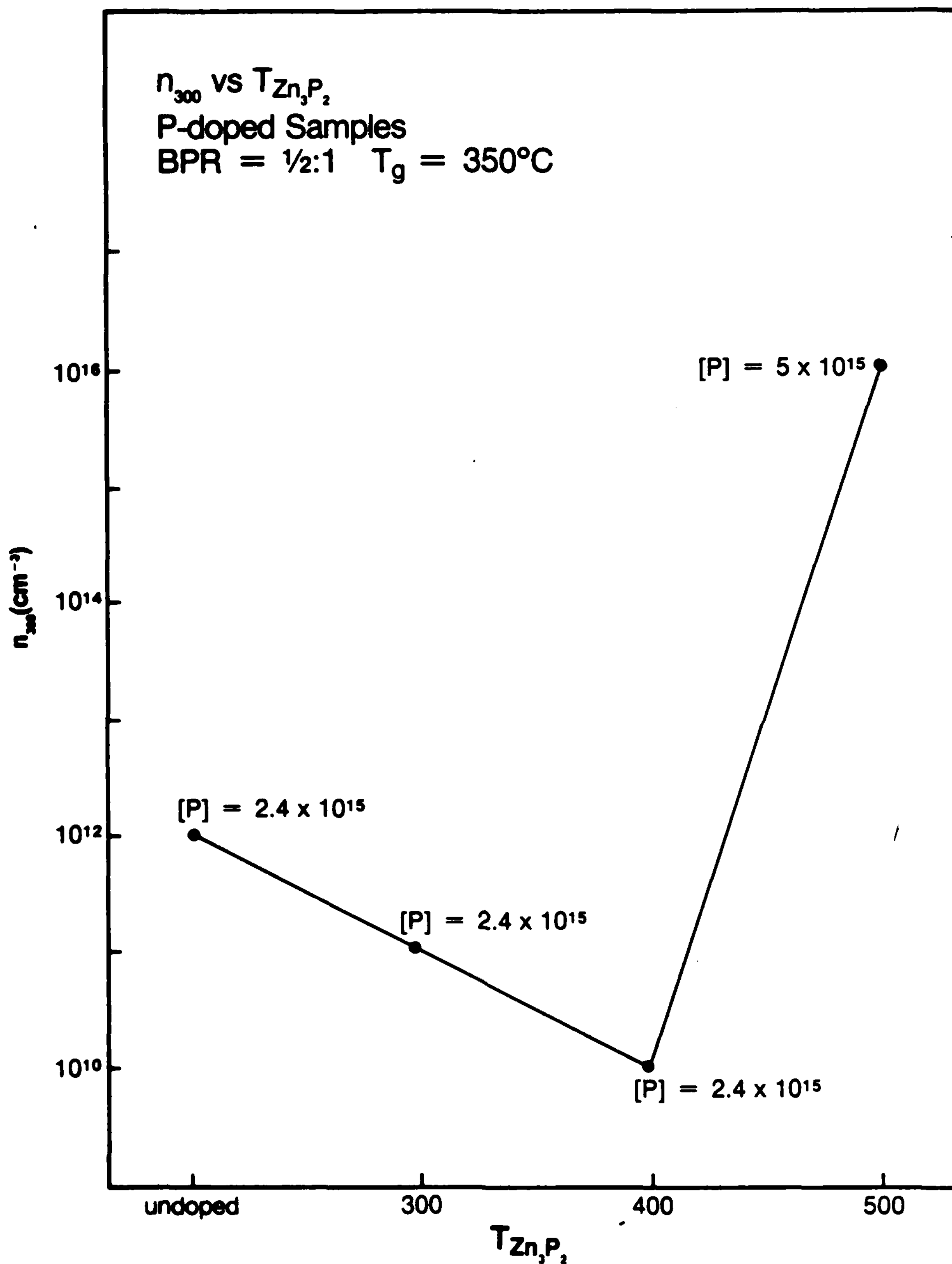

Figure 2-23. Room temperature electron concentration plotted as a function of Zn_3P_2 oven temperature.

ZSE85A, ZSE80A, ZSE84A, and ZSE86A were grown with T_g=350°C, T_{ZnP}=500°C, and BPR's of 1/4:1, 1/2:1, 1:1, and 2:1, respectively. The carrier concentrations at room temperature and the peak mobilities were measured to be:

SAMPLE	BPR	n_{300} (cm^{-3})	μ_P (cm^2/V-sec)
ZSE85A	1/4:1	0.25×10^{16}	7000
ZSE80A	1/2:1	1×10^{16}	5000
ZSE84A	1:1	0.5×10^{16}	6000
ZSE86A	2:1	$< 10^{14}$	not measured

These results, plotted in Figure 2-24, show no clear relationship between the BPR and electrical characteristics. The three relevant samples had roughly the same carrier concentrations and peak electron mobilities. (The results for ZSE86A are not unexpected since the undoped samples grown under these conditions were always highly resistive.) The third P-doping study investigated the effects of growth temperature. The results shown below and illustrated in Figure 2-25 along with the SIMS results, show that the amount of phosphorous incorporated depends strongly upon substrate temperature.

SAMPLE	T_g (°C)	n_{300} (cm^{-3})	μ_P (cm^2/V-sec)
ZSE82A	270	$<<10^{14}$	not measured
ZSE83A	300	1×10^{15}	1600
ZSE84A	350	5×10^{15}	6000

Using arguments similar to those presented for the Na-doped samples, it is seen that the concentration of acceptors increases with decreasing substrate temperature faster than does the donor concentration, but the change in carrier concentration is small. It appears that P can be incorporated into ZnSe, but P is not a promising candidate for p-type doping. From the study in which the substrate temperature was varied, it can be seen that the carrier concentration was changed by less than 5×10^{15} cm^{-3} with the incorporation of > 10^{17} cm^{-3} P atoms. This indicates that P may be going in as a deep level.

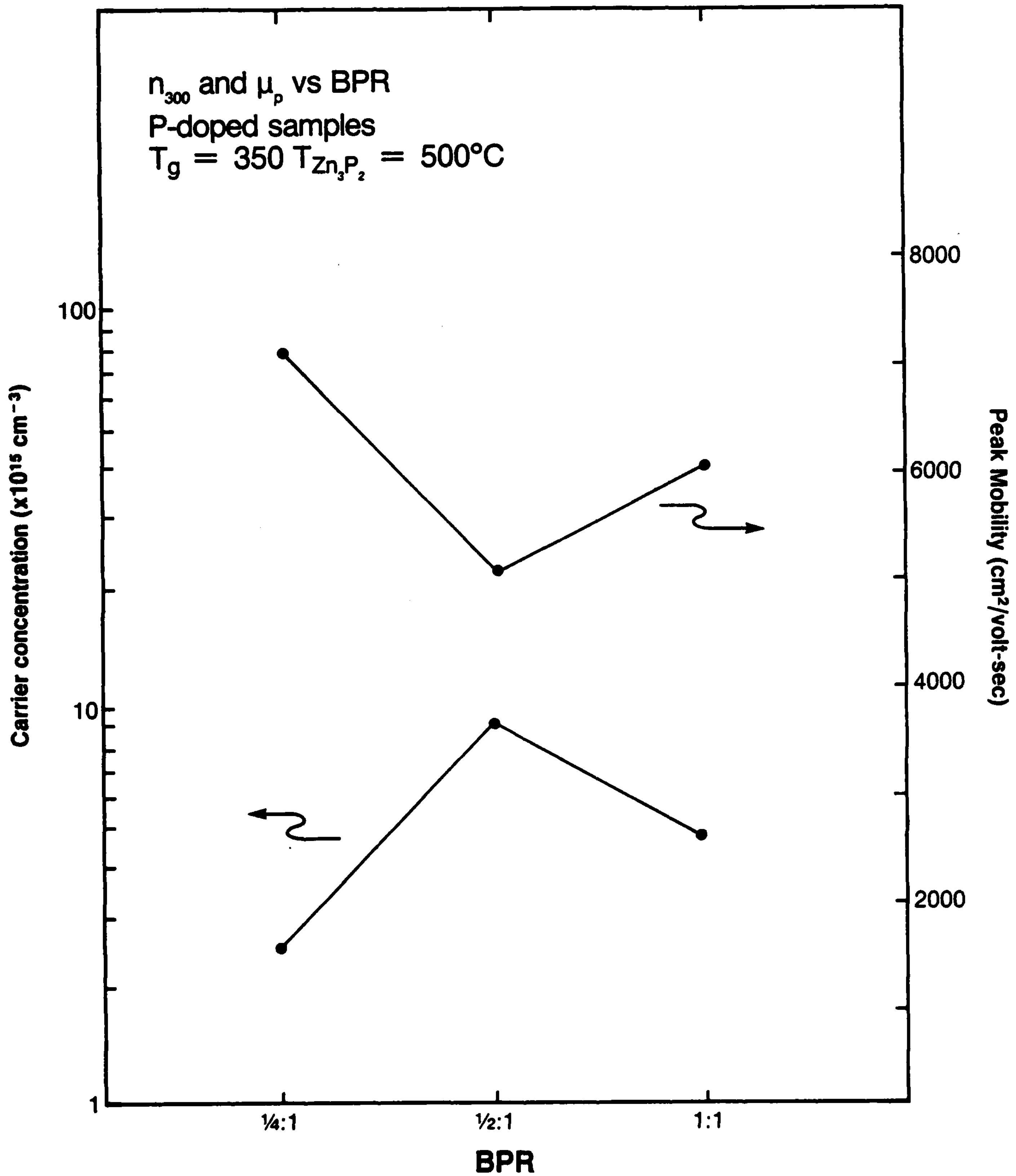

Figure 2-24. Carrier concentration and peak mobility of P-doped layers plotted as a function of BPR for constant T_g and P flux.

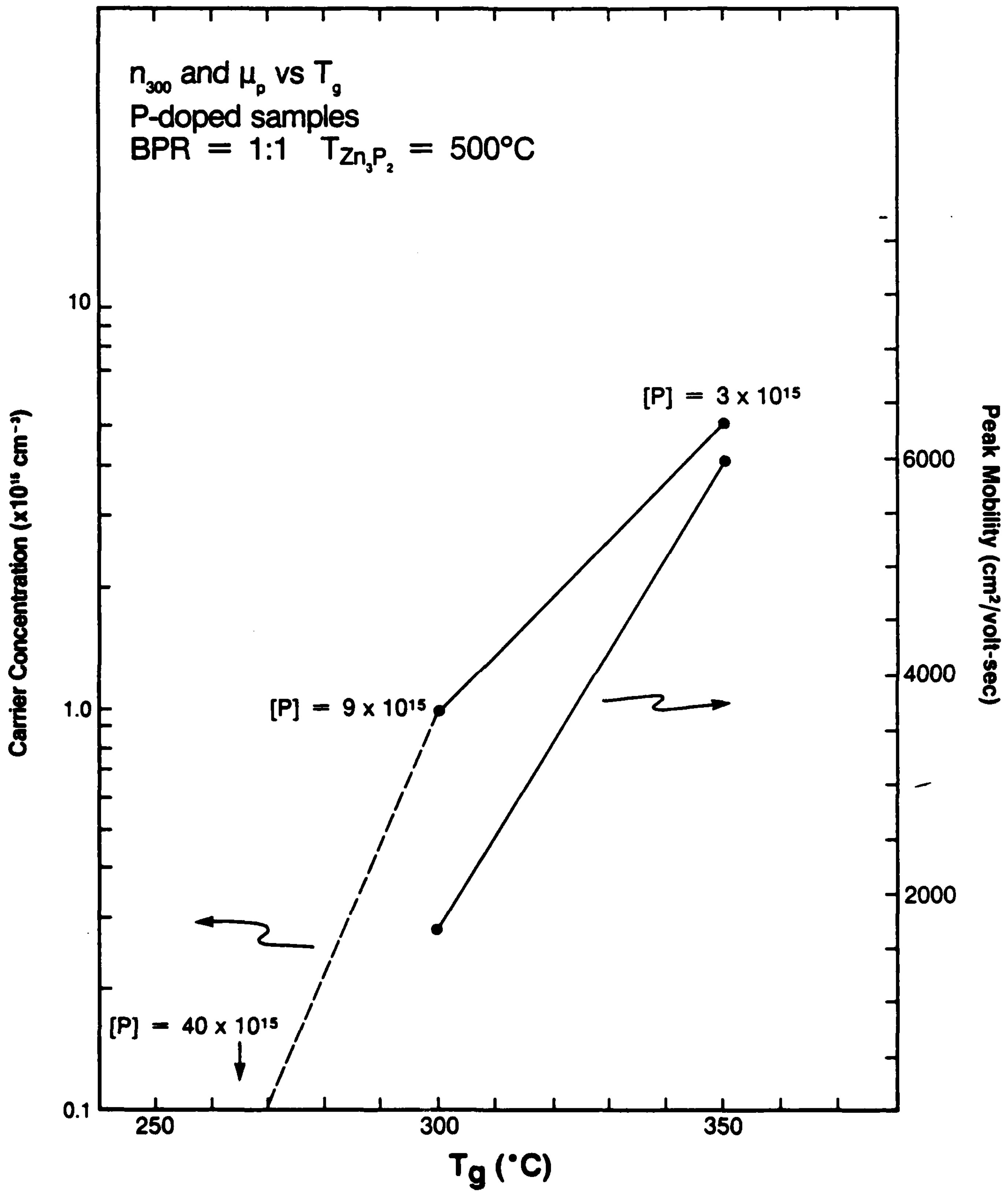

Figure 2-25. Carrier concentration and peak mobility of P-doped layers plotted as a function of T_g for constant BPR and P flux.

2.3 Project 2, Task 1: Device Research - Photopumping, e-Beam Pumping and Cavity Formation

2.3.1 e-Beam Pumping Measurements

During the past quarter we have used electron-beam excitation to examine the cathodoluminescence (CL) from several ZnSe films grown by organometallic vapor phase epitaxy (OMVPE) by Prof. Bruce Wessels of Northwestern University. We have successfully pumped some of these films to lasing; this is the first report of lasing in transversely-pumped ZnSe OMVPE films. We were interested in comparing the lasing properties of these materials to those of our MBE-grown films. We found the lasing thresholds in the MBE films to be lower than those of the OMVPE films by factors ranging from 2.5 to 10, depending on the particular film and cavities used. While we originally felt we were seeing an inverse correlation between the intensity of the near-band-edge (NBE) PL emission and the lasing threshold, our recent experiments do not support such a conclusion. Figure 2-26, for example, shows the light output-versus-e-beam current density characteristics for a 4.3 μm -thick MBE film (ZSE48A) and a 6.2 μm-thick OMVPE film (Y141). While the NBE emission intensities are similar for these two films, the threshold for the OMVPE film is approximately 2.5 times higher. Cavities cleaved from a 4.5 μm-thick OMVPE film (Y143) had an average threshold current density of about 9 A/cm^2. Currently, we believe that differences in the surface quality between the two types of films may account for the differences in the observed lasing thresholds. Under 200X magnification in an optical microscope, the surface of the OMVPE films was found to exhibit a coarse, grainy texture, while the MBE films were smooth and featureless at this magnification. The increased cavity losses due to the rough surface morphology in the case of the OMVPE films may account for the higher thresholds.

Further evidence for the absence of a correlation between large NBE emission intensity and small lasing threshold is seen in Figure 2-27 where we show the light output-versus-e-beam current density for another cavity formed from ZSE48A and one from a recently-grown MBE sample ZSE88A (4.75 μm thick). This latter sample was grown using the new 6N+ Se source material. As was demonstrated in the photoluminescence discussion in this report, its NBE emission intensity was reduced by a factor of approximately 20 from that of a sample such as ZSE48A. Nonetheless, as Figure 2-27 demonstrates, the lasing threshold is nearly identical to that of ZSE48A.

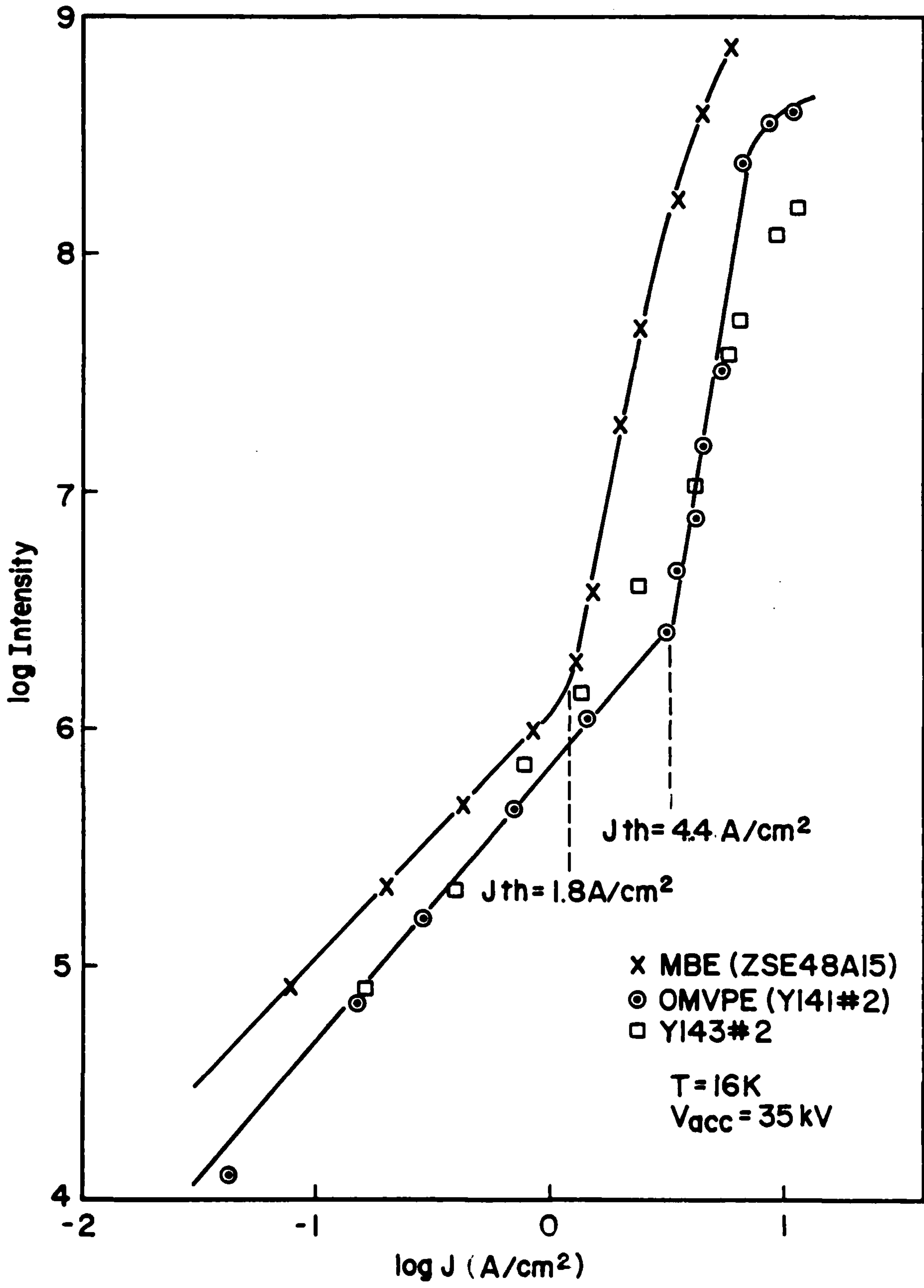

Figure 2-26. Light output of e-beam pumped laser versus e-beam current density.

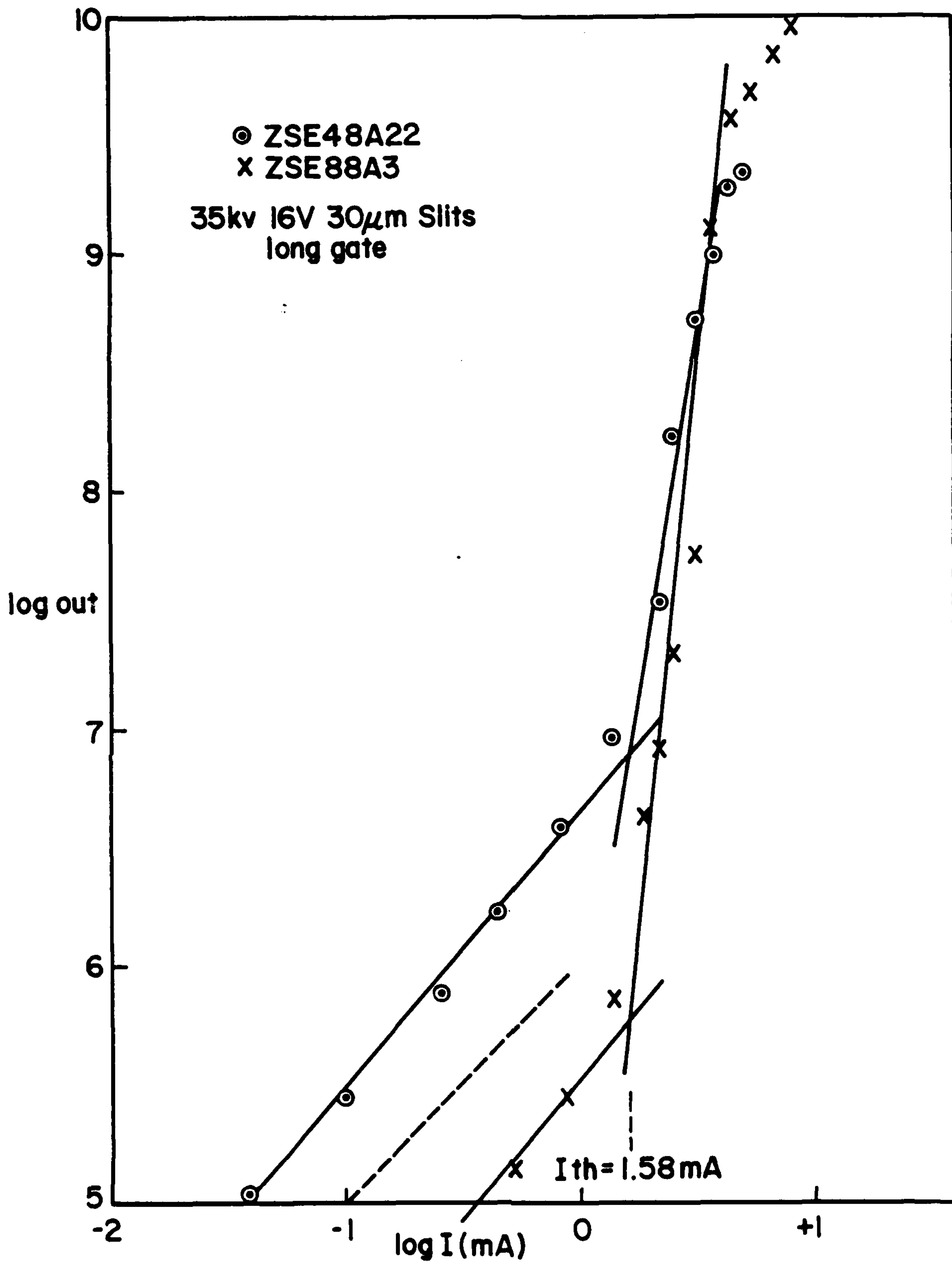

Figure 2-27. No correlation between large NBE emission intensity and small lasing threshold is seen in this plot of light output versus e-beam current. Dashed line has a slope of +1.

The lower spontaneous emission intensity from ZSE88A for $J < J_{th}$ causes the onset of lasing to appear more dramatic in this case (note the five orders of magnitude rise in the output intensity at threshold for ZSE88A compared to only three orders of magnitude for ZSE48A). The lasing occurs at approximately the same wavelength in the two cases. Figure 2-28 shows that at low e-beam current densities ($J \ll J_{th}$), the (CL) spectra for both samples are dominated by a feature believed to be due to the inelastic scattering of excitons by electrons (446 nm in Figure 2-28). The ZSE88A spectrum is much weaker, as expected from the much smaller NBE emission intensity. In addition, the ZSE48A spectrum contains distinct narrow peaks due to radiative decay of excitons bound to neutral donors (443.1 nm) and an LO-phonon overtone of this process (447.9 nm). Because of the substantial reduction of the extrinsic donor concentration brought about by the use of the 6N+ Se, these lines are nearly absent from the CL spectrum of ZSE88A, as they were from the NBE PL emission spectrum.

We are developing techniques to evaporate metal mirror coatings to the end facets of the laser cavities so that we can reduce our lasing thresholds by increasing the mirror reflectance. Up to this point we have relied on the natural (Fresnel) reflectance of the cleaved semiconductor-air interface to provide optical feedback for the cavity.

In addition, we expect to be able to demonstrate optically-pumped lasing action in these MBE-grown films by the end of the next quarter.

2.4 Project 2, Task 2: Contact Studies

2.4.1 Electron Transport Across GaAs-ZnSe Interface

For certain optoelectronic devices, it is necessary to inject charge carriers from the substrate. This implies that the substrate provides an injecting contact without any interfacial barrier between the substrate and the active layer. In this quarter, we have investigated electron injection from n^+-GaAs into ZnSe.

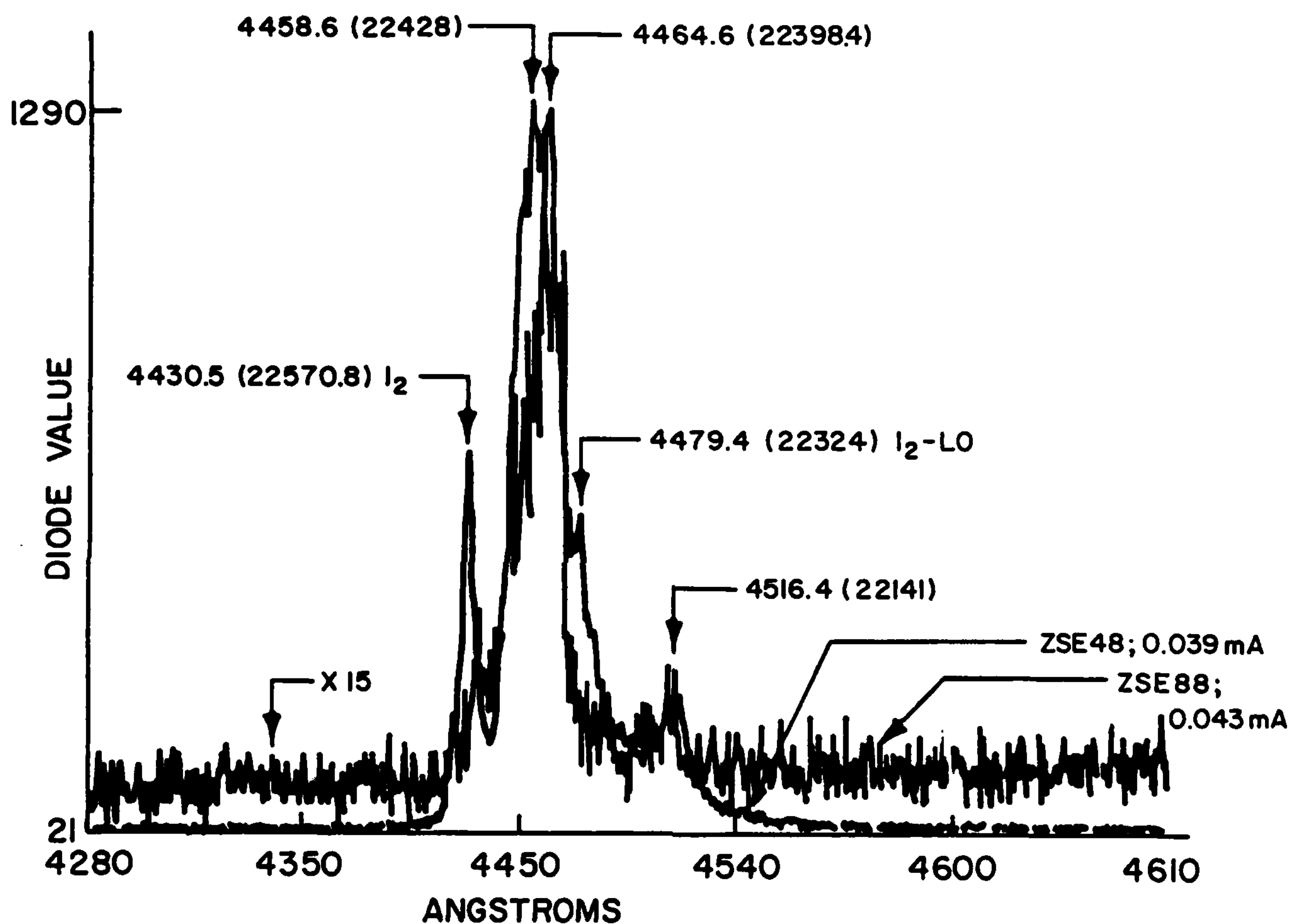

Figure 2-28. At low e-beam current densities, the CL spectra for both ZSE88A and ZSE48A are dominated by a feature believed to be due to inelastic scattering of excitons by electrons (446 nm peak).

Earlier (Quarterly Technical Progress Report #1, July 1986), we reported current-voltage (I-V) characteristics on Schottky barrier (SB) structures on ZnSe (SB/ZnSe/n^+-GaAs). Forward bias current was always lower than what one would expect from ideal SB structures. Based on Anderson's electron affinity rule ($\Delta E_c = X_{ZnSe} - X_{GaAs} = 0.02$ eV) one expects very small interfacial conduction band discontinuity, ΔE_c (0.02 eV). However, resistivity values obtained from large forward bias I-V characteristics were two to three orders of magnitude higher than the resistivity values obtained from Hall measurements.

It has been known that surface state density on ZnSe is lower than III-V materials. In the latter, the Fermi level is pinned by high surface density and Schottky barrier height in III-V semiconductors is independent of metal work function. Therefore, Anderson's rule and surface state density should not account for the low forward bias current. This seems to indicate that low forward bias current is due to either a native oxide on ZnSe surface (current will be limited by transport through the oxide) or due to a larger conduction band discontinuity between ZnSe and GaAs.

In order to prove some of the above hypotheses, planar Schottky barrier structures on ZnSe/SI GaAs were fabricated. In this case, gold Schottky barrier was evaporated on ZnSe and subsequently indium ohmic contact was formed by annealing In at 300°C. I-V characteristics indicated an ideality factor n ~ 1.1. Moreover, a much higher forward current (~ 1 mA) was observed in this structure.

For comparison, measurements were made on transverse geometry with current transport through the ZnSe/n^+-GaAs interface. The results are shown in Figure 2-29. The transverse structure showed two orders of magnitude lower forward current than the planar geometry.

The results suggest that interface band discontinuity is largely responsible for the low forward bias current observed in SB structures.

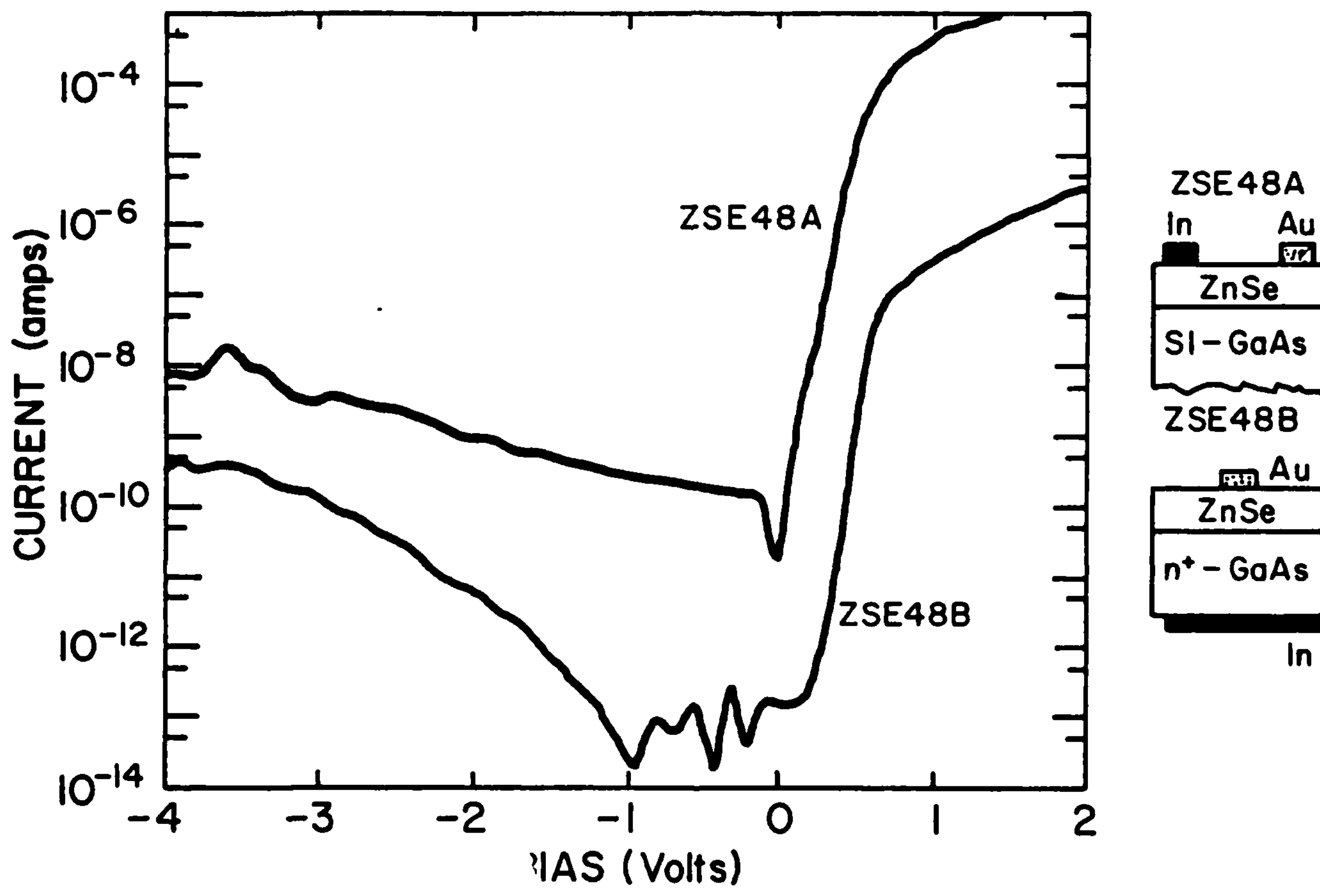

Figure 2-29. Current-voltage characteristics of gold Schottky barriers on ZnSe. (Potential of Au with respect to In.)

Planar and transverse measurements were made on ZnSe on n^+ GaAs substrate. The results are summarized in Figure 2-30. Curve 1 indicates negative polarity of In for the forward bias current. This is qualitatively in agreement with the hypothetical band diagram shown in the inset of Figure 2-30. Forward I-V characteristics shown in curves 2 and 3 indicate negligible contributions of current from n^+-GaAs. Curve 4 shows reduced forward current because of the interfacial barrier between ZnSe and GaAs.

In order to obtain interfacial barrier height, temperature dependence of I-V measurements have been made on In/ZnSe/n^+-GaAs/In structure. The results were analyzed based upon the thermionic emission model given below.

$$j = AT^{1/2}\exp\left(\frac{-q\phi}{kT}\right) \times \exp\left(\frac{qV}{kT}\right) = j_o \exp\left(\frac{qV}{kT}\right)$$

where j is the current, A is a constant, T is the temperature, ϕ is the barrier height and V is the applied voltage assumed to be entirely dropped across ZnSe. A plot of $\ln(j_o/T^{1/2})$ versus 1/T gives a barrier height, ϕ of 0.4 $\pm$ 0.2 eV. We are currently trying to repeat experiments to reduce the scatter in our measurements.

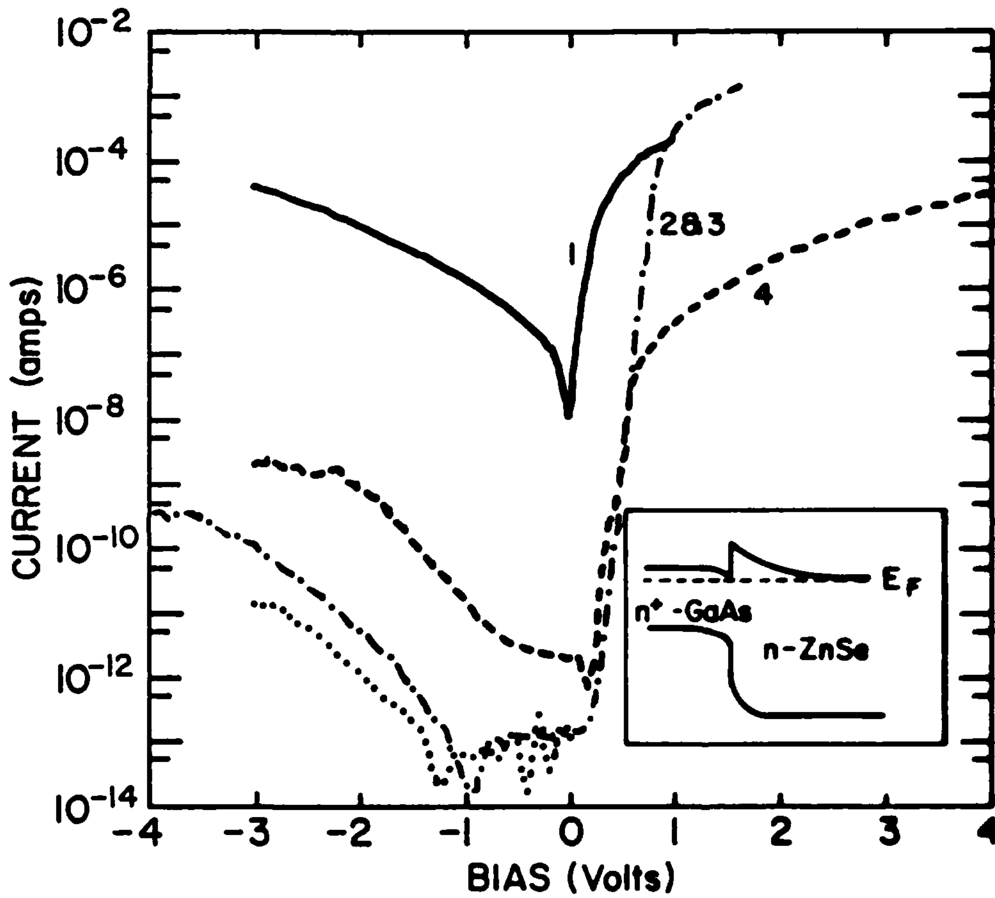

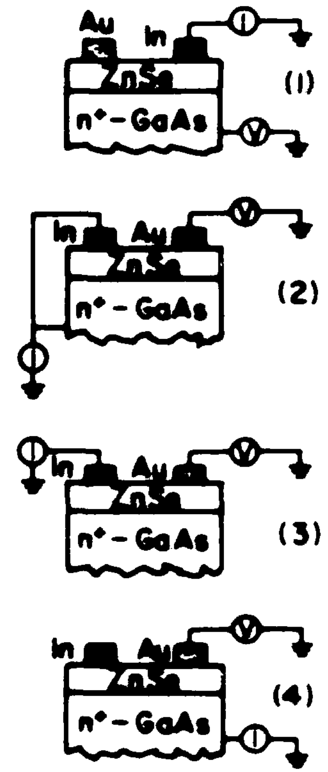

Figure 2-30. Current-voltage characteristics of indium (Ohmic) and gold (Schottky) contacts to ZnSe with current transport through n^+-GaAs and n-ZnSe interface.

3.0 REFERENCES

1. A.G. Cullis, N.G. Chew, and J.I. Hutchinson, Ultramicroscopy 17, 203 (1985).

2. K. Rajan, R.L. Devine and W.T. Moore (1987) to be published.

3. S.J. Rodner, S.M. Kooh, and J.S. Harris, Jr., Appl. Phys. Lett. 49(26), 1764 (1986).

4. J. Kleiman, R.M. Park, and S. Qadri, J. Appl. Phys., 6 (1987).

5. R.M. Park, J. Kleiman, and H.A. Mar, SPIE Conference, Bay Point, Florida, (1987).

6. F.A. Ponce, W. Stutius, and J.G. Werther, Thin. Sol. Films, 104, 133 (1983).

7. J.O. Williams, A.C. Wright, and T. Yao, Phil. Mag. A 54(4), 553 (1986).

8. T. Yao and Y. Okada, Jpn. J. Appl. Phys., 25, 821 (1986).

END
7-87
DTIC